

Department of Environment Systems

Graduate School of Frontier Sciences

The University of Tokyo

2020

Master's Thesis

**Fluoride Transport and
Adsorption/desorption Processes with
Different Flow Rates**

Submitted January 20, 2021

Adviser: Professor Tokunaga Tomochika

Co-Adviser: Professor Tabeta Shigeru

Wanyi ZHAO

TABLE OF CONTENT

ACKNOLEDGEMENTS	4
LIST OF NOMENCLATURE	5
LIST OF TABLES	6
LIST OF FIGURES	7
I. INTRODUCTION	9
1.1 BACKGROUND.....	9
1.1.1. FLUORIDE	9
1.1.2 FLUORIDE IN SOIL.....	9
1.1.3 FLUORIDE IN GROUNDWATER.....	10
1.1.4 FLUORIDE AND HUMAN HEALTH.....	11
1.1.5 DEFLUORIDATION	12
1.2 OBJECTIVES	13
1.3 STRUCTURE OF THE THESIS.....	13
II. MECHANISM OF FLUORIDE SORPTION AND TRANSPORT IN SOIL.....	14
2.1 FLUORIDE SORPTION MECHANISM	14
2.1.1 ISOTHERM MODELS	14
2.1.2 SURFACE COMPLEXATION MODELS.....	15
2.2 FLUORIDE TRANSPORT IN SATURATED SOIL	20
2.2.1 DIFFUSION.....	20
2.2.2 ADVECTION	21
2.2.3 DISPERSION	21
2.2.4 ADVECTION-DISPERSION EQUATION (ADE)	22
2.3 NONEQUILIBRIUM TRANSPORT PROCESSES	23
1) CHEMICAL NONEQUILIBRIUM PROCESS	23
2) PHYSICAL NONEQUILIBRIUM PROCESS.....	23

III. NUMERICAL SIMULATIONS OF THE EXPERIMENTAL DATA.....	26
3.1 DESCRIPTION OF THE EXPERIMENT TO BE ANALYZED	26
3.1.1 COLUMN EXPERIMENTS WITH FLOW INTERRUPTION	26
3.1.2 DESCRIPTION OF THE LABORATORY EXPERIMENT	27
3.2 NUMERICAL SIMULATION PROCEDURE	28
3.2.1 CONCEPTUAL MODEL.....	28
3.2.2 MODEL DESCRIPTION	30
3.2.3 GEOCHEMICAL TRANSPORT CODE PHREEQC	30
3.2.4 PROCEDURE FOR USING PHREEQC FOR MODELING TRANSPORT WITH SORPTION PROCESS	31
3.2.4 VALIDATION OF THE NUMERICAL MODEL	34
IV. RESULTS	36
4.1 SIMULATION RESULTS.....	36
V. DISCUSSIONS	50
5.1 COMPARATION BETWEEN THE MODEL AND THE EXPERIMENTAL DATA	50
5.2 MODIFIED CASES	51
VI. CONCLUSION	54
6.1 SUMMARY	54
6.2 IMPLICATIONS	54
6.3 FUTURE WORK AND RECOMMENDATIONS	55
APPENDIX.....	56
REFERENCES	57

ACKNOWLEDGEMENTS

Foremost, I cannot express enough gratitude to my supervisor Prof. Tokunaga Tomochika, who supported me throughout my master's study. His patient guidance, encouragement, and advices inspired me and give me confidence. I am really thankful for the chats at the end of our meetings which always enlighten me with new perspectives of questions that puzzled me as well as a more profound understanding on science. I am extremely grateful for all of the opportunities I was given to further my research and the personal support during the coronavirus pandemic, without which I cannot finish my study here.

I sincerely thank my co-advisor Prof. Tabeta Shigeru for his valuable time, his encouragement, and insightful suggestions that help me sharpen my thinking and improve my research from other perspectives.

I am deeply grateful to Prof. Otomo Junichiro for his continuous help and support during my exchange program, his kindness and consideration helps me through the hardest times in London.

I am hugely indebted to Dr. Sakambari Padhi, who is so generous to share her knowledge and precious time with me. Her selfless support, her patience for my questions regardless of her own busy schedule kept me going when I was stuck. I also enjoyed exchanging the ideas on cultural with her. Her diligence and toughness really encourage me a lot. I see her as a friend and a mentor.

Special thanks to my brilliant labmates for the discussions, the all-time interesting but sometimes harsh feedbacks which pushed me to really think hard of my works, and happy distractions to rest my mind outside of stress. I am so grateful for their help in every aspect during my staying here.

I shall forever give thanks to my family and all my friends for always being there for me, giving me suggestions, encouraging me to overcome the obstacles and making me happy.

Finally, I would like to dedicate this work to my parents for their unconditional support and unparalleled love. It is their support that makes me the person who I am and their love that gives me the courage to believe in the future and looking up at the stars even in the darkest times. I feel so lucky to start my life journey with being their daughter.

LIST OF NOMENCLATURE

Symbols

- C_m is the concentration of solute in the immobile regions (ML^{-3})
 C_{im} the concentration of solute in the immobile regions (ML^{-3})
 v_m : the average pore-water velocity in the mobile region (LT^{-1})
 D_m : coefficient of longitudinal hydrodynamic dispersion in the mobile region (L^2T^{-1})
 θ : volumetric water content (L^3L^{-3})
 θ_m : volumetric mobile water content (L^3L^{-3})
 θ_{im} : volumetric immobile water content (L^3L^{-3})
 ρ_b : dry soil bulk density (ML^{-3})
 s : the solid phase concentration of total solute (MM^{-1})
 s_m : the solid phase concentration of solute from the mobile region per mass of dry soil (MM^{-1})
 s_{im} : the solid phase concentration of solute from the immobile region per mass of dry soil (MM^{-1})
 α : mass transfer coefficient between mobile and immobile region (T^{-1})
 z : distance (L)
 t : time (T)
 K_d : distribution coefficient (L^3M^{-1})
 K_F : Freundlich coefficient (L^3M^{-1})
 K_L : Langmuir coefficient (L^3M^{-1})
 σ : surface charge density (NL^{-1})
 Ψ_o : surface potential (V)
 ε_o : permittivity of vacuum

Abbreviations

- ADE: advection-dispersion equation
PNE: physical nonequilibrium
SCM: surface complexation model
BTC: breakthrough curve

LIST OF TABLES

Table 3.1 Ion concentration and pH of ICEFIELD water (data
source:<https://store.shopping.yahoo.co.jp/icefieldwater/4582153131061.html>).

Table 3.2 Parameters for the model, from Padhi, (2015).

Table 4.1 A schematic of analyzing logic.

Table 5.1 Parameters used for the fitting with experimental data.

LIST OF FIGURES

Figure 1.1 World map showing the location and the connection of different fluoride belts with high fluoride concentration. From Chowdhury *et al.* (2019).

Figure 1.2 Sources of fluoride in the environment. From Edmunds and Smedley, (2013).

Figure 2.1 Distribution of ions at the surface. (a) is showing the difference between inner-sphere and outer-sphere complexes, (b) shows different planes of the surface where complexes are formed. “s” is surface functional groups; “a” and “ β ” for inner-sphere and outer-sphere complexes, respectively; “d” represents the ions in the diffuse layer. Stumm (1992).

Figure 2.2 Representative elementary volume from Parkhurst and Appelo (1999).

Figure 2.3 (a) A schematic of the Two-region model, adapted from Van Genuchten and Wierenga (1976); Fesch *et al.* (1998). (b) and (c) An enlarged illustration for (a), modified from Tanahashi *et al.* (1994).

Figure 3.1 Simulation result of BTC with flow interruption. Modified after Brusseau *et al.* (1997)

Figure 3.2 Schematic of setups for column experiment .

Figure 3.3 A schematic of the conceptual model.

Figure 3.4 Logic of modeling using PHREEQC based on experiment procedures.

Figure 3.5 PHREEQC calculation process for transport modeling, drawn based on Parkhurst and Appelo (1999).

Figure 3.6 The concept of PHREEQC stagnant zone with reactions, drawn based on Parkhurst and Appelo (1999).

Figure 3.7 Comparison of the analytical solution and numerical result using.

Figure 4.1 Fluoride relative concentration in the mobile zones versus pore volume with different flow rates. With no sorption and advection-dispersion with physical nonequilibrium transport process.

Figure 4.2 Fluoride relative concentration in the mobile zones versus pore volume with different flow rates. With advection-dispersion transport and different sorption processes.

Figure 4.3 Fluoride relative concentration in the mobile zones versus pore volume linear and surface complexation sorption processes on breakthrough curves with physical nonequilibrium transport at different flow rates.

Figure 4.4 Fluoride relative concentration in the mobile zones versus pore volume with physical nonequilibrium transport process on breakthrough curves with linear sorption at different flow rates.

Figure 4.5 Fluoride relative concentration in the mobile zones versus pore volume with surface complexation model at different flow rates.

Figure 4.6 Mobile/immobile zone concentration at high/low flow rate till 50 pore volume with physical nonequilibrium transport process and surface complexation model for sorption process.

Figure 4.7 Mobile/immobile zone concentration at high/low flow rate till 300 pore volume with physical nonequilibrium transport process and surface complexation model for sorption process.

Figure 4.8 Fluoride relative concentration in the mobile zones versus pore volume at different flow rates. Immobile zone is included in transport and surface complexation model for sorption process.

Figure 4.9 Fluoride relative concentration in the immobile zones versus pore volume at different flow rates. Immobile zone is included in transport and surface complexation model for sorption process.

Figure 4.10 Fluoride relative concentration versus pore volume at different immobile zone ratios a high flow rate.

Figure 4.11 Fluoride relative concentration versus pore volume at different immobile zone ratios a high flow rate.

Figure 4.12 Fluoride relative concentration in the mobile/immobile zones versus time at different flow rates and different immobile zone ratio, sorption explained by the surface complexation model.

Figure 5.1 A comparison between the model and the experimental data.

Figure 5.2 Fluoride relative concentration versus pore volume at different magnitude of the exchange factor α .

Figure 5.3 Experimental data fitting with immobile ratio=0.15.

Figure 5.4 Experimental data fitting with exchange factor $\alpha=1.32 \times 10^{-5}$ and immobile ratio equals to 0.15.

I. INTRODUCTION

1.1 Background

1.1.1. Fluoride

Fluorine is the lightest element of the halogen group and the most electronegative element that usually exists as fluoride which constitutes about 0.06-0.09 percent of the earth's crust. (Hem, 1985).

Fluoride exists in minerals such as fluorspar, cryolite and fluorapatite (Murray, 1986). Fluoride ions have the same charge and almost same radius with OH^- so it can substitute each other in minerals (Hem, 1985). In some parts of the world, for example, Afghanistan, China, Central Africa, Japan, Iraq, and India. fluoride concentrations are higher than those in other parts across the globe and locally high concentration can be found in most part of the world (WHO, 2011). Countries that fluoride concentration is higher can be divided into five global fluoride belts connecting each other geologically and geographically (Chowdhury *et al.*, 2019) (Figure 1.1).

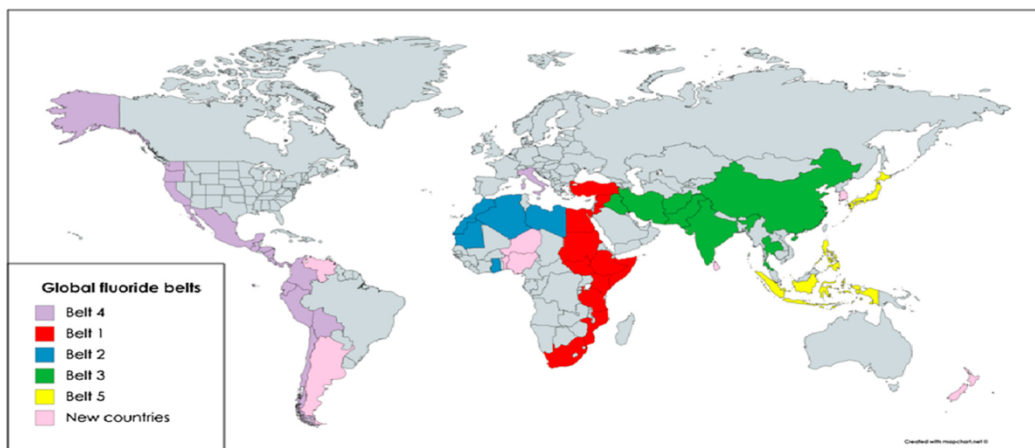


Figure 1.1 World map showing the location and the connection of different fluoride belts with high fluoride concentration. From Chowdhury *et al.* (2019).

1.1.2 Fluoride in soil

Average fluoride concentration in soils is approximately 200-400 mg/kg (Fuge and Andrews, 1988) and can be high as 20000mg/kg locally in some high-fluoride areas (Edmunds and Smedley, 2013). High soil fluoride concentration can harm grazing animals by mixing up with feed (Cronin *et al.*, 2017) and can induce aluminum and iron release from soil (Polomski *et al.*, 1982)

Fluoride in soil can be originated from nature sources or accumulated through anthropogenic activities. Natural soil fluoride can derive from minerals such as fluorapatite ($\text{Ca}_5(\text{PO}_4)_3\text{F}$),

fluorite (CaF_2), cryolite (Na_3AlF_6), topaz ($\text{Al}(\text{SiO}_4)\text{F}_2$), and micaceous clay minerals (Pickering, 1966). Fluoride content differs according to soils due to multiple reasons, such as different soil parent materials and tectonics of the area. Soils that consist of high amounts of fluoride bearing minerals often reported to have a greater fluoride content in a range of about 7–38 g/kg (Smith *et al.*, 1977). Anthropogenically, fluoride in soil comes from phosphate mining, phosphate fertilizers (Maadid *et al.*, 2017); aluminum smelters and pesticides (Cronin *et al.*, 2017), and sewage sludges (Rea, 1979).

Atmospheric and surface water can also be the source of fluoride into the soil (Figure 1.2). Marine aerosols, volcano ash, industrial emissions such as coal burning, and aluminum smelting can deposit fluoride into soil either directly or by rainfall.

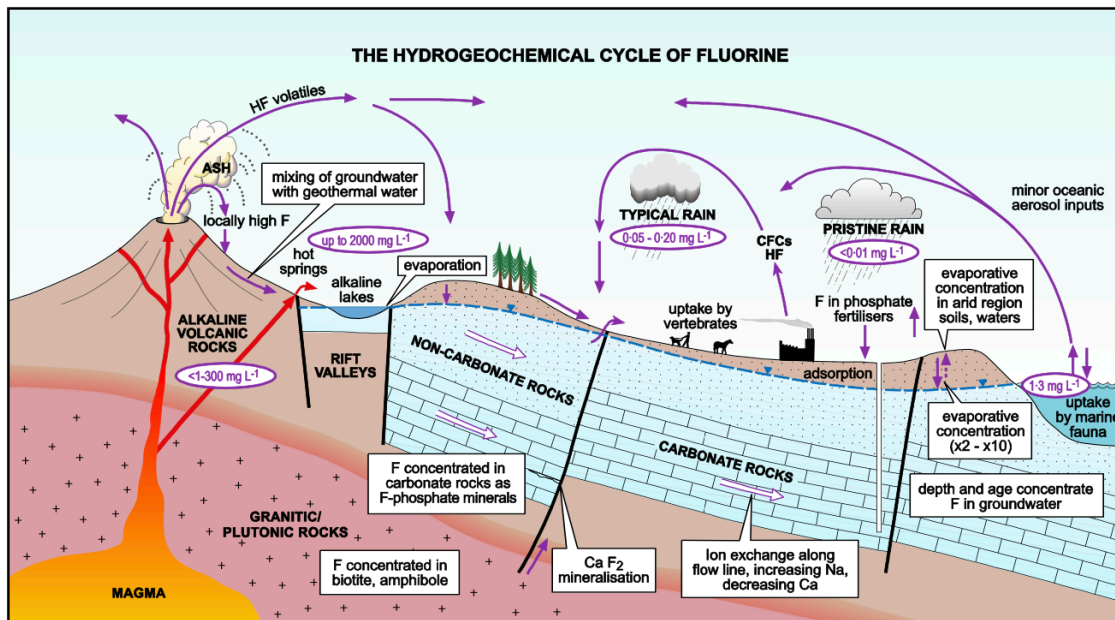


Figure 1.2 Sources of fluoride in the environment. From Edmunds and Smedley, (2013)

Amount of fluoride adsorption in soil is different with soil types and especially depends on pH. Fluoride exists as F^- in soil and form complexes with Al or H and form complexes like AlF_2^+ (Padhi and Tokunaga, 2018). According to Edmunds and Smedley (2013), amount of fluoride uptake by acidic soils can ten times larger than that of alkaline soils.

1.1.3 Fluoride in groundwater

Fluoride can leach into groundwater by processes such as water-rock reactions between fluoride rich minerals and water bodies, and desorption from fluoride-rich soils. Many natural factors are related to fluoride concentration in groundwater. Regions where climate is arid or semiarid are prone to be more fluoride enriched in groundwater due to less precipitation and

higher evaporation or evapotranspiration that condense the solute (Chowdhury *et al.* 2019). The flow rates of groundwater in these regions are also slow enough to extend the duration of water-rock reactions (Smedley *et al.*, 2002). If the duration of reaction is longer, groundwater with fluoride will residence longer in the host aquifer, which can also result in high fluoride concentration. Deeper groundwater probably more concentrate in fluoride than shallow groundwater or surface waters that are frequently replenished (Edmunds and Smedley, 2013).

Tectonics also affects groundwater fluoride concentration. As shown in Figure 1.1, many counties locating on the fluoride belts also rich in volcanic activities and geothermal sources such as western USA and Japan. Ash from eruption contains high amount of fluoride that can be infiltrated into groundwater with rainfall. High weathering of volcanic soils due to high altitude of volcanos can also be one explanation for fluoride enriched groundwater (Chowdhury *et al.* 2019).

Rock types play a significant part. Granitic rocks are especially related to high fluoride concentrations (Chikte *et al.* 2001; WHO,2002) because minerals that constitute granitic rocks are abundant in fluoride, for example, micas, amphiboles, and apatite (Edmunds and Smedley, 2013).

In many developing countries, people depend on exploiting groundwater to drink, which is not treated appropriately due to economical or technical limitations. Different standards are set for fluoride in drinking waters. For example, fluoride concentration regulated by WHO guideline (2011) is 1.5mg/L. Long-term intake of high-fluoride water will cause chronic endemic fluorosis (WHO, 2002).

1.1.4 Fluoride and human health

Studying how fluoride affects human body can date back to the late 19th century when chemists first noticed that different fluoride contains in human bones and teeth (Edmunds and Smedley, 2013).

Drinking water is usually considered the major pathway for fluoride intake, while it is worth noticing that food and beverages such as seafood, specific kinds of teas, wines and juices can also account for dietary input (Jackson *et al.*, 2002b). Toothpaste with fluoride contents is also a crucial source (Ozsvath, 2009). During digestion, fluoride exists as HF^0 complex under the environment of low pH in the stomach, adsorbed from the stomach and small intestine through diffusion and eventually transported to mucosa with higher pH, where HF^0 complex is ready to be dissociated and release fluoride ions (Whitford and Pashley, 1984). After indigestion, most fluoride involves in the progression of teeth and bone formation and the remaining amount is excreted through urine (Cerklewski, 1997).

Researches have indicated that fluoride can help reduce dental caries and may have a positive effect on preventing osteoporosis (Bernstein *et al.*, 1966). Fluoride can be beneficial for skeleton strengthening if taken at appropriate dose: as a major component in bone formation, hydroxyl ions in the crystal lattice of hydroxyapatite ($(\text{Ca}_{10}(\text{PO}_4)_6(\text{OH})_2)$ or $\text{Ca}_5(\text{PO}_4)_3\text{OH}$) can be substituted by fluoride ions, which lead to a reduction in volume per cell unit, the density increases, also chemical stability is largely enhanced. Thus, the structure of bones gets strengthened (Aoba, 1997). As for teeth, fluoride can boost the mineral stability of tooth minerals by participating in the equilibrium between tooth surface and oral fluids (Chow, 1990).

Fluoride has acute toxicity if accidentally taken, such as from toothpastes or pesticides, and may have symptoms such as vomiting, bronchospasm and sometimes even lead to death (Shulman *et al.*, 1997). For adverse effects, overdosing of fluoride can cause dental fluorosis, which can be identified by mottling tooth surfaces or enamel with white horizontal bands. In some serious cases, the white part grows to yellow or even black patches and finally the color changes stop with tooth porosity increment, which means structural damages and lead to crispy teeth (Nagendra, 2003). Osteosclerosis is another disease caused by excessive intake of fluoride. The symptoms are pain and stiffness in the joint and bones with increasing bone density. Fluoride also has neurological effects, a study in China shows that children were underperformed in the intelligence test when they digested more fluoride than regular (Wang *et al.*, 2007). Likewise, in the advanced stage of osteosclerosis, in company with deformation of spine and major bones, paralysis, neurological defects occur, too (Ozsvath, 2009).

1.1.5 Defluoridation

Because many countries on the fluoride belt are categorized as developing countries, the remediation processes are preferred to be cheaper, easy to operate, and more sustainable (Singh *et al.*, 2018).

Defluoridation methods can be classified into three groups: 1. Using sorption media such as activated alumina, activated carbon and bone charcoal that are packed in a column or bucket to adsorb fluoride. This method is cheap, easy to construct and of high removal efficiency, but problem lies with monitoring and renewing of adsorbent (Fawell *et al.*, 2006). Also, in some cultures, people refuse to use bone product because religious belief (Tekle-Haimanot *et al.*, 2006). 2. Co-precipitation method, by adding chemicals such as lime, gypsum, and aluminum sulfate to form flocculation or sedimentation to reduce the high concentration on a daily basis. The most established method is the Nalgonda technique (Nawlakhe and Bulusu, 1989), which removes fluoride by adding aluminum chloride, lime (or sodium aluminate) and bleaching powder into the water container, stirring the water and then wait till precipitation forms. This method is low-cost, is simple, and can be applied both at small (bucket) and large (village water defluorination plants)

scales (Edmunds and Smedley, 2013). The disadvantage is that the chemicals for precipitation need to be added daily and generate sludge, which may become a secondary fluoride sink unless treated properly (Fawell *et al.*, 2006). 3. Contact precipitation methods, developed by WHO in 2006, by adding calcium and phosphate into water before it enters a catalyst filter bed which is pre-saturated with F^- . Fluoride will precipitate as CaF_2 or fluorapatite (Dahi, 1996). Comparing to the co-precipitation methods, this produces no sludge, and can be used for a larger community (Fawell *et al.*, 2006).

Other methods such as using biological agents (Mondal *et al.*, 2013), reverse osmosis and nanofiltration with specific membrane (Richards, *et al.*, 2010) are also highly efficient in defluoridation but more expensive for massive utilization in developing countries.

Before defluoridation, people often use pumps to extract groundwater and pumping rate may result in a mixing between deep (old) groundwater with high concentration and shallow (young) groundwater with low concentration (Edmunds and Smedley, 2013). The possible mixing of old high-fluoride groundwater may contaminate young groundwater and become a new source for upper aquifer.

Also, in contaminant remediation procedure, “pump and treat” is a common way to remove fluoride from soil. The efficiency of these methods using pumps can be affected by pumping rate, higher pumping rate means higher flow rate in the soil. In order to understand how fluoride sorption behavior is impacted by flow rate, the following objectives are set.

1.2 Objectives

- 1) To develop a numerical model describing fluoride adsorption/desorption and transport behaviors and compare the result with laboratory experiments;
- 2) To investigate fluoride adsorption/desorption and transport behaviors at different flow rates.

1.3 Structure of the thesis

This thesis is organized as follows: Chapter 1 is a general introduction of fluoride in soil and groundwater, toxicity to human health from summarized literature survey of previous studies; Chapter 2 contains mechanism of fluoride sorption and transport in soil, and the basic theories for the mathematical model followed; Chapter 3 describes the details for numerical approach and compared with result from laboratory experiments; Chapter 4 presents several numerical simulation results of fluoride sorption and transport with different parameters; Chapter 5 discusses the simulation results and Chapter 6 summarizes the findings and recommendations for future research.

II. MECHANISMS OF FLUORIDE SORPTION AND TRANSPORT IN SOIL

2.1 Fluoride sorption mechanism

The sorption mechanism can be explained by different kinds of models: isotherm models such as the K_d model, the Langmuir-Freundlich model or the surface complexation models.

2.1.1 Isotherm models

An isotherm is the relationship between sorbed and dissolved solute concentration at a certain given temperature at equilibrium condition (Appelo and Postma, 2004).

1) Linear K_d model

The K_d model describes the relationship between the concentration of solid and liquid in a linear expression as:

$$s = K_d \cdot c \quad (2.1)$$

where K_d is the distribution coefficient (m^3/kg), s is the concentration of solute that adsorbed on to the adsorbent (mol/kg) and c the concentration of solute in the solution (mol/L). The values of K_d are usually obtained empirically and are assumed to be constant throughout the sorption process. Thus, although the model can be easily coupled with mass transport equations (Bethke and Brady, 2000), its application is limited to specific conditions such as a fixed pH and cannot explain the experiment results well (Goldberg *et al.*, 2007). The K_d model is not based on the mass balance on the sorbing sites, instead, it assumes the sorbent can sorb infinite solute without saturation, which also leads to its failure in explaining ion competition (Valocchi *et al.* 1981).

2) Langmuir and Freundlich isotherms

The Langmuir and Freundlich isotherms were introduced about 100 years ago and are still used frequently because of their simplicity, flexibility, and effectiveness for fitting various experimental data. Many modifications have been proposed from these two isotherms, for example, multisite Langmuir isotherm, the Redlich-Peterson isotherm, and others (Kinniburgh, 1986). Compared to the linear K_d model, these isotherms can describe competitive adsorption and heterogeneity (Kinniburgh, 1986)

① The Freundlich isotherm is defined as:

$$s = K_F \cdot c^n \quad (2.2)$$

where s is the sorbed concentration (mol/kg), c is the solute concentration (mol/L), K_F and n are adjustable parameters. n is usually less than 1, which means the sorbed concentration increases

less than the solute concentration. The Freundlich isotherm assumes an infinite number of sorption sites (Appelo and Postma, 2004)

②Langmuir isotherm

Langmuir isotherm is derived from the law of mass action and the general form is (Goldberg *et al.*, 2007):

$$S = \frac{K_L b \cdot c}{1 + K_L \cdot c} \quad (2.3)$$

Where b is the maximum adsorption capacity of the substrate (kg/kg, etc.), and K_L is the constant describing the strength of solute that bound to the substrate (m^3/kg , etc.) The Langmuir isotherm includes an upper limit of the sorption sites and can also be applied for gas sorption. Although the model is more theoretical based than the Freundlich isotherm, it is still empirical based.

2.1.2 Surface complexation models

Unlike the above mentioned two models, surface complexation models are more theoretical based by including surface charges resulting from protonation, dissociation reactions, and surface complexation reactions at mineral surfaces. The surface complexation models are capable of applying in a wide range of conditions (Goldberg, 1992).

2.1.2.1 Common characteristics of surface complexation models

The models are established based on three common characteristics: the balance of surface charge; electrostatic potential terms, and adjustable parameters (Goldberg, 1992).

1) The balance of surface charge can be explained as:

$$\sigma_H + \sigma_{is} + \sigma_{os} + \sigma_d = 0 \quad (2.4)$$

where σ_H ($\sigma_H = \{ \equiv \text{SOH}_2^+ \} - \{ \equiv \text{SO}^- \}$) is the net proton charge (eq/kg), σ_{is} is the inner-sphere charge, σ_{os} the outer-sphere charge and σ_d is the dissociated charge, SOH_2^+ the protonated surface functional groups and SO^- the deprotonated surface functional groups. Figure 2.1 shows schematics of inner-sphere and outer-sphere complexes:

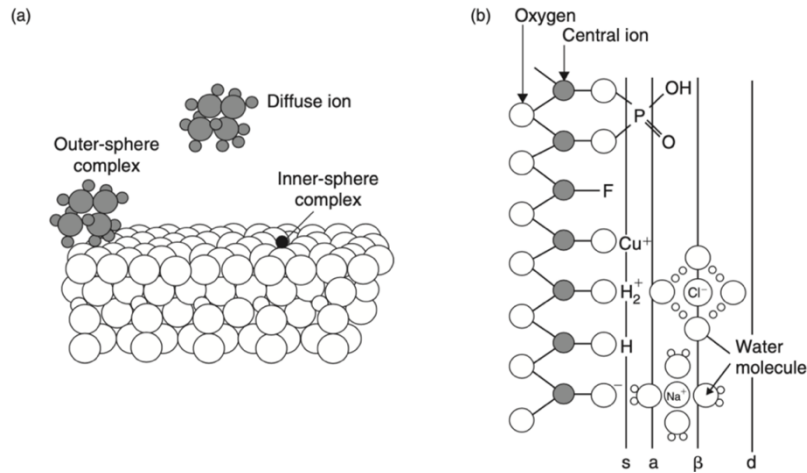


Figure 2.1 Distribution of ions at the surface. (a) is showing the difference between inner-sphere and outer-sphere complexes, (b) shows different planes of the surface where complexes are formed. “s” is surface functional groups; “a” and “β” for inner-sphere and outer-sphere complexes, respectively; “d” represents the ions in the diffuse layer. Stumm (1992)

Outer-sphere complexes are mainly formed by alkali metals and acid anions which have a hydration water shell while inner-sphere complexes mainly with structural oxygens with protons and heavy metals.

2) Electrostatic potential terms

At least one Coulombic correction factor is needed in a surface complexation model to describe the surface charge. This is because the activity of surface species cannot be simply related to the concentration when surface charges are involved. Sposito (1983) explained that when the environment is charge-free or neutral, the activity coefficient is unity if the surface complex fully covers the surface. However, the actual case is different, so the electrostatic potential terms are necessary to be introduced. The expression is:

$$e^{-F\Psi_i/RT} \quad (2.5)$$

where Ψ_i is the surface potential (V) in the i th surface plane, F is the Faraday constant (C/mol), R is the molar gas constant (J/mol · K), T is the absolute temperature (K).

3) Adjustable parameters

Mass balance and charge balance for each different surface site and surface plane are defined explicitly in the surface complexation models. All models have these parameters: the equilibrium constant K , the capacitance density for i th surface plane C_i , and, total number of reactive surface hydroxyl groups $[\text{SOH}]_T$ (Goldberg, 1992).

2.1.2.2 Common surface complexation models for fluoride sorption

Two of the most often used models are the constant capacitance model and the generalized two-layer model (Appelo and Postma, 2004).

1) Constant capacitance model (CCM)

Developed by Schindler and Stumm and their team (1987), it assumes the charged surface to be balanced by a parallel layer of counter ions just like a parallel plate condenser, so the relation between surface charge (σ , mol/L) and surface potential (ψ , V) is linear:

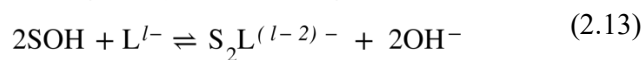
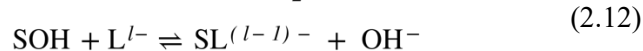
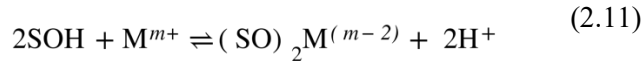
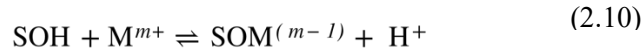
$$\sigma = \frac{CSa}{F} \psi \quad (2.6)$$

where C is the capacitance density (F/m²), S is the specific area (m²/kg), a is the suspension density (kg/m³).

This model is also based on two more assumptions: i) all surface complexes are inner-sphere complexes and mechanism for anion adsorption is ligand exchange; ii) no complexes are formed with the ions in the background electrolyte. Thus, the balance of surface charge is simplified into equation 2.7 and Figure 2.2 is a schematic representation of the surface-solution interface in the constant capacity model.

$$\sigma = \sigma_H + \sigma_{is} \quad (2.7)$$

The surface complexation reaction in the constant capacitance model is (Hohl *et al.*, 1980):



where SOH is the surface functional group, M is the metal ion, m^+ is the charge on the metal ion; L is a ligand and l^- is the charge on the ligand. According to these, the intrinsic conditional equilibrium constants are (Hohl *et al.*, 1980):

$$K_+(\text{int}) = \frac{[\text{SOH}_2^+]}{[\text{SOH}][\text{H}^+]} e^{\frac{F\psi}{RT}} \quad (2.14)$$

$$K_-(\text{int}) = \frac{[\text{SO}^-][\text{H}^+]}{[\text{SOH}]} e^{-\frac{F\psi}{RT}} \quad (2.15)$$

$$K_M^1(\text{int}) = \frac{[\text{SOM}^{m+}][\text{H}^+]}{[\text{SOH}][\text{M}^{m+}]} e^{\frac{(m-1)F\psi}{RT}} \quad (2.16)$$

$$K_M^2(\text{int}) = \frac{[(\text{SO})_2\text{M}^{(m-2)}][\text{H}^+]^2}{[\text{SOH}]^2[\text{M}^{m+}]} e^{\frac{(m-2)F\psi}{RT}} \quad (2.17)$$

$$K_L^1(\text{int}) = \frac{[\text{SL}^{(l-1)-}][\text{OH}^-]}{[\text{SOH}][\text{L}^{l-}]} e^{-\frac{(l-1)F\psi}{RT}} \quad (2.18)$$

$$K_L^2(\text{int}) = \frac{[\text{S}_2\text{L}^{(l-2)-}][\text{OH}^-]^2}{[\text{SOH}]^2[\text{L}^{l-}]} e^{-\frac{(l-2)F\psi}{RT}} \quad (2.19)$$

Two more equations are needed to solve the equilibrium problem: the mass balance for surface functional group:

$$[\text{SOH}]_T = [\text{SOH}] + [\text{SOH}_2^+] + [\text{SO}^-] + [\text{SOM}^{(m-1)}] + [(\text{SO})_2\text{M}^{(m-2)}] + [\text{SL}^{(l-1)-}] + [\text{S}_2\text{L}^{(l-2)-}] \quad (2.20)$$

and the charge balance (Sigg and Stumm, 1981):

$$\begin{aligned} \sigma = & [\text{SOH}_2^+] + (m-1)[\text{SOM}^{(m-1)}] + (m-2)[(\text{SO})_2\text{M}^{(m-2)}] \\ & - [\text{SO}^-] - (l-1)[\text{SL}^{(l-1)-}] - (l-2)[\text{S}_2\text{L}^{(l-2)-}] \end{aligned} \quad (2.21)$$

2) Generalized two-layer model

Dzombak and Morel (1990) developed a generalized two-layer model based on the diffuse layer model proposed by Stumm and co-workers (Stumm *et al.*, 1970; Huang and Stumm, 1973). The diffuse double layer model is based on a theory that instead of a sudden stepped change, the distribution of counterions is changing as their distance from the surface increasing. This change is called the Gouy-Chapman diffuse double layer (Appelo and Postma, 2004).

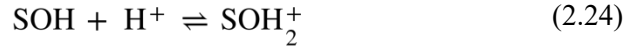
Like the constant capacity model, the two-layer model assumes that all surface complexes are inner-sphere complexes, and no surface complexes are formed with the ions in the background electrolyte. It has two unique assumptions: i) the surface is represented by two layers of planes and ii) The relation between surface charge (σ , mol/L) and surface potential (ψ , V) is expressed as (Dzombak and Morel, 1990):

$$\psi_a = \psi_d \quad (2.22)$$

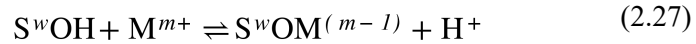
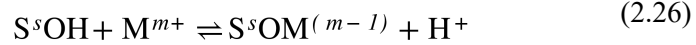
$$\sigma_d = \left(8RT\epsilon\epsilon_0 c \times 10^3 \right)^{1/2} \sinh\left(\frac{Z\psi F}{2RT}\right) \quad (2.23)$$

where R is molar gas constant (8.314 J/mol · K), T the absolute temperature (K), ϵ the dielectric constant of water, ϵ_0 the permittivity of free space (8.854 × 10⁻¹² C/V · m), and c is the molar electrolyte concentration.

The surface reactions for the generalized two-layer model share the same equations with the constant capacity model for protonation and dissociation:

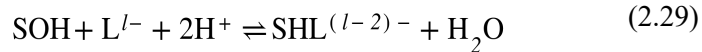
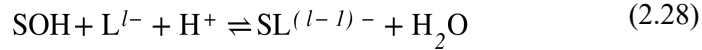


It considers two types of sites with different affinity and metal ion adsorption: a small set of high-affinity strong sites and a large set of low-affinity weak sites. So, the reaction for metal ions is (Goldberg,1992):



where s indicates the high-affinity strong sites and w the low-affinity weak sites.

For ligand exchange reactions, it is not necessary to differentiate site types and the reactions are (Goldberg,1992):



The intrinsic conditional equilibrium constant for the generalized two-layer model is the same with CCM except for ligand exchange:

$$K_L^1(\text{int}) = \frac{[\text{SL}^{(l-1)-}]}{[\text{SOH}][\text{L}^{l-}][\text{H}^+]} e^{\frac{-(l-1)F\Psi}{RT}} \quad (2.30)$$

$$K_L^2(\text{int}) = \frac{[\text{SHL}^{(l-2)-}]}{[\text{SOH}][\text{L}^{l-}][\text{H}^+]^2} e^{\frac{-(l-2)F\Psi}{RT}} \quad (2.31)$$

Mass balance and surface charge balance equations are defined separately; for metal ions:

$$[\text{S}^s\text{OH}]_T = [\text{S}^s\text{OH}] + [\text{S}^s\text{OH}_2^+] + [\text{S}^s\text{O}^-] + [\text{S}^s\text{OM}^{(m-1)}] \quad (2.32)$$

$$[\text{S}^w\text{OH}]_T = [\text{S}^w\text{OH}] + [\text{S}^w\text{OH}_2^+] + [\text{S}^w\text{O}^-] + [\text{S}^w\text{OM}^{(m-1)}] \quad (2.33)$$

$$\sigma = \frac{F}{Sa} \{ [\text{S}^s\text{OH}_2^+] + [\text{S}^w\text{OH}_2^+] + (m-1)[\text{S}^s\text{OM}^{(m-1)}] + (m-1)[\text{S}^w\text{OM}^{(m-1)}] - [\text{S}^s\text{O}^-] - [\text{S}^w\text{O}^-] \} \quad (2.34)$$

and for ligand exchange:

$$[\text{SOH}]_T = [\text{SOH}] + [\text{SOH}_2^+] + [\text{SO}^-] + [\text{SL}^{(l-1)-}] + [\text{SHL}^{(l-2)-}] \quad (2.35)$$

$$\sigma = \frac{F}{Sa} \{ [\text{SOH}_2^+] - [\text{SO}^-] - (l-1)[\text{SL}^{(l-1)-}] - (l-2)[\text{SHL}^{(l-2)-}] \} \quad (2.36)$$

The generalized two-layer model serves as a concise metamodel that can be applied in a variety of scenarios. Although it can be modified to be more complicated ones, the good fitting with many observations indicates such complex model may not be necessary (Dzombak and Morel, 1990).

2.2 Fluoride transport in saturated soil

Transport in porous media is studied by considering the flux of solute into and out of a fixed elemental volume within the flow domain called a “representative elementary volume” (Parkhurst and Appelo, 1999). Differential equations are established based on the conservation of mass into and out of this volume:

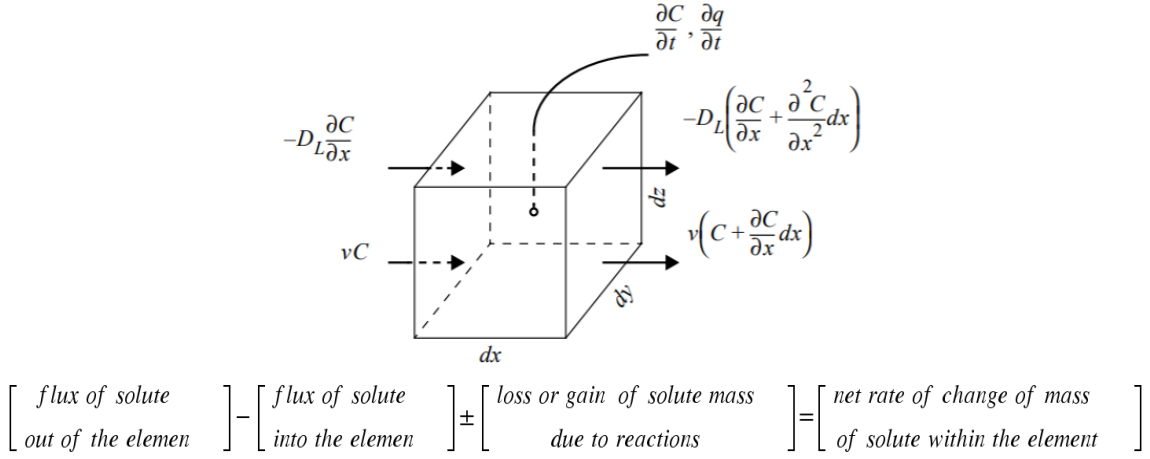


Figure 2.2 Representative elementary volume from Parkhurst and Appelo (1999)

The physical processes that control the flux into and out of this elemental volume are advection and hydrodynamic dispersion. The loss and gain can be due to chemical, biological, or radioactive decay reactions (Freeze and Cherry, 1979).

2.2.1 Diffusion

Mass transfer in water happens wherever there is a concentration gradient. It means even if the fluid is static, the random Brownian movement of solute molecules will not stop thus driving the solute to move from greater concentration to smaller concentration. This process is called diffusion and can be described by the Fick's first law. The one-dimensional form of this law is:

$$F = -D_d \frac{dC}{dx} \quad (2.37)$$

where F is the mass flux of the solute per unit area per unit time, D_d is the diffusion coefficient (L^2/T); C is the concentration of solute (M/L^3); dC/dx is the concentration gradient ($M/L^3/L$). The negative sign indicates that the movement opposes the concentration gradient.

For a pure water system where the concentration is time dependent, Fick's second law is applied, and the one-dimensional form is:

$$\frac{\partial C}{\partial t} = D_d \frac{\partial^2 C}{\partial x^2} \quad (2.38)$$

where $\partial C / \partial t$ is the change of concentration with time (M/L³/T)

2.2.2 Advection

Advection refers to the solute moving together with the flowing fluid. For one dimensional flow, transport velocity is the average linear velocity v , i.e. $v = Q / \varepsilon A$, where Q is flow rate, A is the unit cross sectional area of the column and ε is effective porosity. It differs from the velocity of each solute molecule moving along the pathway and usually smaller than the latter due to tortuosity.

The one-dimensional mass flux in advection is:

$$F = v \varepsilon C \quad (2.39)$$

thus, advection transport equation is

$$\frac{\partial C}{\partial t} = -v \frac{\partial C}{\partial z} \quad (2.40)$$

2.2.3 Dispersion

1) Mechanical dispersion

Solute molecules do not move identically at the average linear velocity. Some are faster while others are slower. This may be because of the different pore size distribution in a porous medium and leads to a mixing of solute along the flow path. This process is called mechanical dispersion. If the direction is along the flow path, it is called longitudinal dispersion which will dilute the advection front concentration while if it is perpendicular to the flow path, it is called transverse dispersion. In order to describe mechanical dispersion, a parameter named dynamic dispersivity, or dispersivity α (L) is introduced and one-dimensional coefficient of longitudinal mechanical dispersion is $\alpha_L v$, where v is the average linear velocity (L/T).

2) Hydrodynamic dispersion

Usually, molecular diffusion cannot be separated from mechanical dispersion during the movement of fluid and they are combined into a new parameter called hydrodynamic dispersion coefficient of which one dimensional expression is:

$$D_L = \alpha_L v + D_d \quad (2.41)$$

where α_L is longitudinal dispersivity (L); v is the average linear velocity (L/T); D_d is the diffusion coefficient in water (L²/T).

2.2.4 Advection-Dispersion Equation (ADE)

Solute movements in porous media are often described by a classical advection-dispersion equation that assumes an inert solute, i.e., non-interacting solute in a steady water flow regime.

The equations are:

$$\text{Advective transport} = v_i \varepsilon C \, dA \quad (2.42)$$

$$\text{Dispersive transport} = \varepsilon D_i \frac{\partial C}{\partial i} \, dA \quad (2.43)$$

Based on the understanding of advective and dispersive transport, on a certain direction, for example, i , the total mass of solute passing through per unit cross-sectional area per unit time

$$F_i = v_i \varepsilon C - \varepsilon D_i \frac{\partial C}{\partial i} \quad (2.44)$$

becomes:

So the total mass of solute can be expressed as:

i) flow into the element:

$$F_x \, dz \, dy + F_y \, dx \, dz + F_z \, dy \, dz \quad (2.45)$$

ii) out of the element:

$$\left(F_x + \frac{\partial F_x}{\partial x} \, dx \right) dy \, dz + \left(F_y + \frac{\partial F_y}{\partial y} \, dy \right) dx \, dz + \left(F_z + \frac{\partial F_z}{\partial z} \, dz \right) dx \, dy \quad (2.46)$$

iii) the difference between in and out:

$$- \left(\frac{\partial F_x}{\partial x} + \frac{\partial F_y}{\partial y} + \frac{\partial F_z}{\partial z} \right) dx \, dy \, dz \quad (2.47)$$

iv) net rate of change of mass:

$$\varepsilon \frac{\partial C}{\partial t} \, dx \, dy \, dz \quad (2.48)$$

Then, the mass balance equation becomes:

$$\frac{\partial F_x}{\partial x} + \frac{\partial F_y}{\partial y} + \frac{\partial F_z}{\partial z} = - \varepsilon \frac{\partial C}{\partial t} \quad (2.49)$$

Substitute the equation (2.44) into F_i :

$$\left[\frac{\partial}{\partial x} \left(D_x \frac{\partial C}{\partial x} \right) + \frac{\partial}{\partial y} \left(D_y \frac{\partial C}{\partial y} \right) + \frac{\partial}{\partial z} \left(D_z \frac{\partial C}{\partial z} \right) \right] - \left[\frac{\partial}{\partial x} (v_x C) + \frac{\partial}{\partial y} (v_y C) + \frac{\partial}{\partial z} (v_z C) \right] = \frac{\partial C}{\partial t} \quad (2.50)$$

This is the three-dimensional non-reactive solute mass transport equation of steady-state flow. If the porous media is saturated, homogeneous isotropic and the pore velocity is the same throughout the porous media, equation (2.50) can be simplified as the one-dimensional version:

$$\frac{\partial C}{\partial t} = -v \frac{\partial C}{\partial z} + D_L \frac{\partial^2 C}{\partial z^2} \quad (2.51)$$

2.3 Nonequilibrium transport processes

“Nonequilibrium” transport gets its name compared to the ideal equilibrium transport process that is instantaneous without retardation. Attempts have been made to explain these kinds of non-ideal behaviors by constructing physical or chemical-based models.

1) Chemical nonequilibrium process

Chemical nonequilibrium happens due to chemical reactions between solutes and sorbents being relatively slower compared to solute transport. The most commonly applied model is the two-site model that assumes the sorption sites into two types: one on which the sorption is supposed to be instantaneous and the other is considered as time-dependent (Van Genuchten and Wagenet, 1989)

2) Physical nonequilibrium process

In natural heterogeneous porous media, a certain fraction of pores can only be accessed by diffusion. When the concentration in these pores is larger than that in the bulk solute, these stagnant zones will provide an amount of solute that acts as sink/source components affecting transport behavior. Behaviors like this occur not only in sorbing but also conservative solutes, indicating the mechanism of physical nonequilibrium is a transport component rather than a sorption-included process (Brusseau and Rao, 1980). Many conceptual models are used in explaining physical nonequilibrium processes with different water content and solute transport regions (e.g., saturated/unsaturated or inter-aggregates/intra-aggregates) such as the two-region model, the dual-porosity model, the dual-permeability model and other more complex models coupling with other nonequilibrium processes (Šimůnek and van Genuchten, 2008).

The two-region model is often used to describe physical nonequilibrium processes under saturated and inter-aggregates conditions. It divides soil porosity into two regions according to transport regime: a mobile region dominated by advection and an immobile region dominated by diffusion. The immobile region is termed for the relatively stagnant soil water compared to the mobile region (De Smedt and Wierenga, 1979).

The total porosity of the column ε is the sum of both regions: mobile region ε_m and immobile region ε_{im} :

$$\varepsilon = \varepsilon_m + \varepsilon_{im} \quad (2.52)$$

Coats and Smith (1964) were the first to couple the advection-dispersion equation with a first-order mass transfer equation to account for breakthrough curves in their experiment. Based on what was proposed by Deans (1963) which took the amount of stagnant volume and rate constant for mass transfer into consideration, they furthered the model by using differential equations and used a first order mass transfer coefficient to describe solute transfer between two regions. It turned out to fit the experimental data better for explaining mass transfer in dead-end pores. Van Genuchten and Wierenga (1976) further improved this model and developed the general transport equation with sorption process as equations (2.53) to (2.55).

$$\theta_m \frac{\partial C_m}{\partial t} + \theta_{im} \frac{\partial C_{im}}{\partial t} + \rho_b \frac{\partial s}{\partial t} = \theta_m D_m \frac{\partial^2 C_m}{\partial z^2} - v_m \theta_m \frac{\partial C_m}{\partial z} \quad (2.53)$$

$$\theta_{im} \frac{\partial C_{im}}{\partial t} + \rho_b \frac{\partial s_{im}}{\partial t} = \alpha (C_m - C_{im}) \quad (2.54)$$

$$\theta = \theta_m + \theta_{im} \quad \theta_v = \theta_m v_m \quad \theta D = \theta_m D_m \quad s = s_m + s_{im} \quad (2.55)$$

where, C_m is the concentration of solute in the mobile regions (ML^{-3}); C_{im} the concentration of solute in the immobile regions (ML^{-3}); v_m is the average pore-water velocity in the mobile region (LT^{-1}); D_m the coefficient of longitudinal hydrodynamic dispersion in the mobile region (L^2T^{-1}). θ the volumetric water content (L^3L^{-3}), θ_m the volumetric mobile water content (L^3L^{-3}), θ_{im} :volumetric immobile water content (L^3L^{-3}), ρ_b is the dry soil bulk density (ML^{-3}), s the solid phase concentration of total solute. s_m is the solid phase concentration of solute from the mobile region per mass of dry soil (MM^{-1}), s_{im} the solid phase concentration of solute from the immobile region per mass of dry soil (MM^{-1}), α the mass transfer coefficient between mobile and immobile region (T^{-1}), z is distance (L) and t is time (T)

A detailed explanation for the two-region model is shown in Figure 2.4. As water flows into porous media, it can be divided into two regions regarding to the mobility. Most of the water is movable and is called the mobile water. Solute transport into this kind of water by advection and dispersion (bold black arrows in Figure 2.3(a)). The water in dead-end pores is less movable, i.e. the immobile water, solute transport into these water only by diffusion (fine double arrows in Figure 2.3(a)). Soil is also divided into two regions, one region touching with mobile water and

one region touching immobile water. Figure 2.3 (b) is an enlarged illustration for the two-region model. The circles indicate soil particles, and the black bold arrows indicate advection-dispersion, which the majority of solute is transported, and the fine double arrows indicate solute transport by diffusion. Figure 2.3 (c) shows how the soil regions touching with water regions. The fine arrows with one direction indicate mass transfer between the two water regions, which is described by the α in equation (2.54). The fine arrows with two directions indicate the sorption reactions between soil and water.

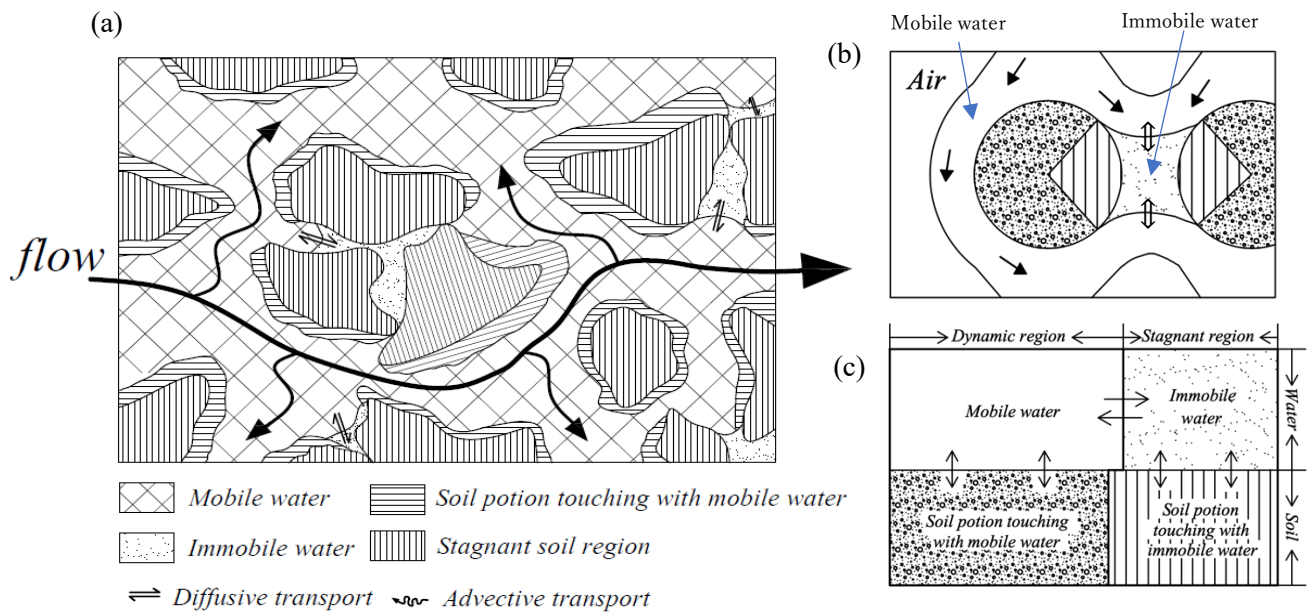


Figure 2.3 (a) A schematic of the Two-region model, adapted from Van Genuchten and Wierenga (1976); Fesch *et al.* (1998). (b) and (c) An enlarged illustration for (a), modified from Tanahashi *et al.* (1994)

III. NUMERICAL SIMULATIONS OF THE EXPERIMENTAL DATA

3.1 Description of the experiment to be analyzed

3.1.1 Column experiments with flow interruption

Column experiments are often used for studying sorption and transport behaviors of solute of interest or characteristics of a specific substrate. The fundamental idea is to pump the liquid containing solute of interest continuously or with certain intermission through a column packed up with certain substrate and then analyze the effluent for specific objectives. The intrinsic characteristics of the substrate is obtained by pumping a conservative tracer and then optimize the result from the breakthrough curve. After getting these parameters, the solute of interest is introduced and analyzed.

Flow interruption technique is basically the same as continuous flow experiments but with additional stop flow events in the leading and tailing fronts of the breakthrough curves. It has been frequently used in previous studies studying sorption behaviors of solutes (e.g., Fesch *et al.*, 1998; Brusseau *et al.*, 1989,1997).

The procedure for conducting column experiments with flow interruptions is as follows. At first, displace the fluid containing solute being studied at a steady flow rate into a water-saturated soil column, stop the flow for a period and reinitiate flow.

The interruption event can be repeated several times according to different objectives and conditions. During the interruption period, based on the two-region model, the bulk solution stops flowing and advective transport in the mobile region ceases. But this stop event provides solutes sufficient time to diffuse out of the mobile zone and into the immobile zone. So the in situ concentration reduces. In the BTC, stop flow event shows a distinguishable difference than that without interruption if physical nonequilibrium exists. The flow interruption method is considered to be more sensitive at detecting physical nonequilibrium process than continuous column experiment (Brusseau *et al.*, 1997). Figure 3.1 shows flow stopped at point A at a relative high concentration when sorption is equilibrated and recommenced at B. The “I” part indicates the residual concentration during interruption, so it is lower than that at point A, “II” part indicates concentration is gradually increasing to that before the stop event. Here, pore volume is the dimensionless time equals to (pore velocity $v \times$ transport time t / column length L).

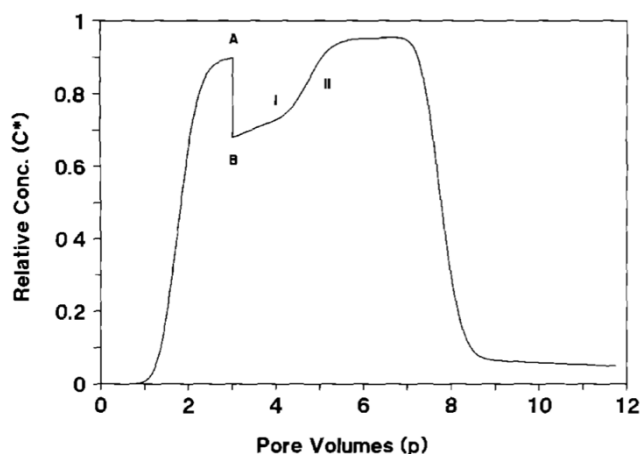


Figure 3.1 Simulation result of BTC with flow interruption. Modified after Brusseau *et al.* (1997)

As discussed previously, physical nonequilibrium is a transport component that also influences nonsorbing solutes. By performing column experiments with stop flow events on both nonsorbing solute and solute of interest and inspecting the BTCs, the dominating nonequilibrium process can be presumed, i.e., if drops during adsorption process and/or rises during desorption exist in the BTC of nonsorbing solute, it is suggested that physical nonequilibrium transport exists. If the BTC of interested solute shows a drop whilst the nonsorbing solute doesn't, it is suggested that sorption process is included in the nonequilibrium mechanism. In this case, whether physical nonequilibrium exists can be determined by fitting the kinetic parameters obtained from the BTC of nonsorbing solute. If the simulation results fit experimental data of the solute of interest well, physical nonequilibrium is considered as the dominating nonequilibrium mechanism (Brusseau *et al.*, 1989).

3.1.2 Description of the laboratory experiment

Laboratory column experiments were conducted by Padhi (2015) at 25 °C. The set-up is shown in Figure 3.2. The column used was 30 cm in length and 6.4 cm in diameter. Acrylic resin was selected as the column material because it is transparent, rigid, and relatively inert to NaF used in the experiments. NaF of 50 mg/L is pumped into the column from the lower side to the upper side. Flow rate is set to 3.6 ml/min (4.55×10^{-5} m/s) and flow interruption is applied at 5.74 pore volume for 12 hours and 11.49 pore volumes for 84 hours. The total adsorption last for 17.5 pore volume. The desorption starts after a few days of adsorption and the ICEFIELD water was used as flushing solution for it has a distinct stable $\delta^{18}O$ and δ^2H , which makes it possible to differentiate from MilliQ water used for adsorption process. The content of ICEFIELD water is listed in table 3.1:

Table 3.1 Ion concentration and pH of ICEFIELD water

Ca²⁺	8.6 mg/L	Mg²⁺	1.5 mg/L
Na⁺	0.86 mg/L	pH	7.0

(data source: <https://store.shopping.yahoo.co.jp/icefieldwater/4582153131061.html>)

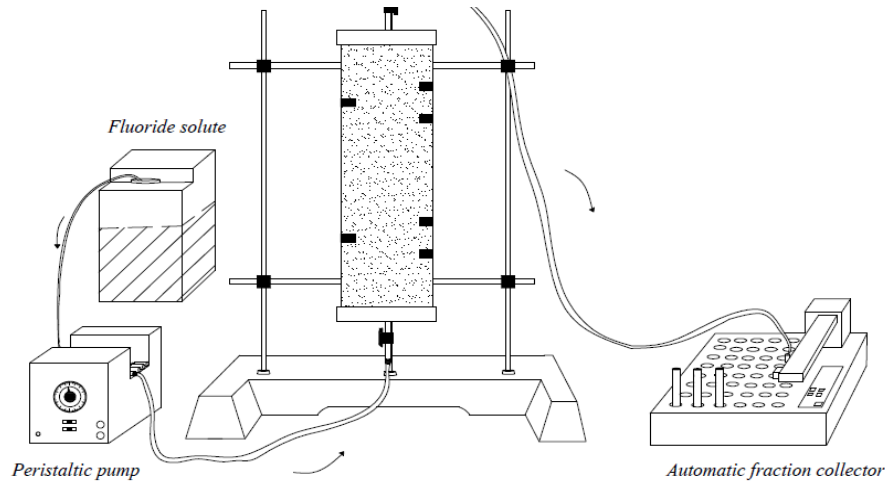


Figure 3.2 Schematic of setups for column experiment

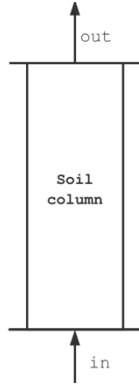
3.2 Numerical simulation procedure

3.2.1 Conceptual model

1) The model is established base on the following considerations (Van Genuchten and Wierenga, 1976):

- ① The soil is homogeneous and isotropic;
- ② The mobile and immobile zones are seen as continua that occupies the whole modeling domain;
- ③ In the mobile zone, the solute is transported by advection, dispersion but only diffusion in the immobile zone. Mass transfer between these two zones is defined by an exchange factor;
- ④ Solute can be adsorbed on both zones and the solute in the liquid is in equilibrium with the solute on the solid, the relationship is described by the surface complexation model.

2) Governing equations for model



Advective transport: $v \cdot \theta \cdot \frac{dC}{dz} \cdot Adz$

Dispersive transport: $-\theta \cdot D \cdot \frac{\partial C}{\partial z} \cdot Adz$

Sorption: $\rho_b \frac{\partial s}{\partial t} Adz$

$$M_{in} - M_{sorption} = M_{out}$$

Mass balance during transport:

Inlet: $M_{in} = \left(v \cdot C - D \frac{\partial C}{\partial z} \right) \theta \cdot Adz$

Outlet: $M_{out} = \left(M_{in} + \frac{\partial M_{in}}{\partial z} dz \right) \theta \cdot Adz$

$$\left(v \cdot C - D \frac{\partial C}{\partial z} \right) \theta \cdot A - \left(M_{in} + \frac{\partial M_{in}}{\partial z} dz \right) \theta \cdot A = \rho_b \frac{\partial s}{\partial t} A + \theta \frac{\partial C}{\partial t} A \quad (3.1)$$

Figure 3.3 A schematic of the conceptual model

The governing equations are: advection-dispersion equation with immobile zones and sorption (details in Eq. 2.58 to 2.60 in Chapter2)

$$\theta_m \frac{\partial C_m}{\partial t} + \theta_{im} \frac{\partial C_{im}}{\partial t} + \rho_b \frac{\partial s}{\partial t} = \theta_m D_m \frac{\partial^2 C_m}{\partial z^2} - v_m \theta_m \frac{\partial C_m}{\partial z}$$

$$\theta_{im} \frac{\partial C_{im}}{\partial t} + \rho_b \frac{\partial s_{im}}{\partial t} = \alpha (C_m - C_{im})$$

$$\theta = \theta_m + \theta_{im} \quad \theta_v = \theta_m v_m \quad \theta D = \theta_m D_m \quad s = s_m + s_{im}$$

3) Boundary conditions

The upper boundary condition for inlet is the constant concentration boundary with a fixed NaF concentration of 50 mg/L of fluoride, and the lower boundary for outlet is a flux boundary.

4) Parameters

The parameters used for the model are listed in Table 3.2, which were obtained by experiments and optimized by CXTFIT (Toride and Van Genuchten, 1995)

Table 3.2 Parameters for the model, from Padhi, (2015)

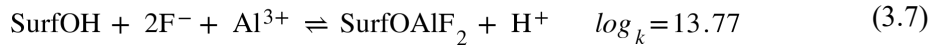
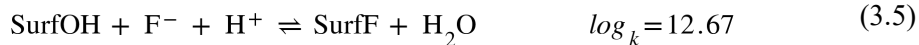
Parameter	Value	Unit
Column length	30	cm
Total porosity	0.39	
Dispersion coefficient	8.9×10^{-7}	m ² /s
Mass transfer coefficient	1.32×10^{-3}	s ⁻¹
Mobile water fraction	0.76	
Surface site density	9.3×10^{-2}	moles/L
Surface area	7.67	m ² /s
Influent pH	7	

3.2.2 Model description

Fluoride transport with sorption process was modeled with different flow rates.

First, for transport, physical nonequilibrium process is described by the two-region model. The immobile and mobile zone are assumed to have the same diffusion properties and the exchange factor (or mass transfer coefficient s^{-1}) is set as 1.32×10^{-3} from previous research (Padhi, 2015). The porosity in each mobile cell and immobile cell is 0.28 and 0.11, respectively, calculated from the product of total porosity and mobile/immobile fractions from Padhi (2015). In this model, 60 mobile and 60 immobile cells are defined. The number 60 is chosen because the soil column is 30cm in length and will thus result in a grid size equal to $30\text{cm}/60 = 5 \times 10^{-3}$ m, which is relatively easy to calculate and satisfy the requirement for avoiding numerical dispersion.

Second, for sorption process, a diffuse double layer model (Dzombak and Morel, 1990) is used. The surface reaction used for fluoride adsorption/desorption is (Padhi, 2015):



The adsorption process starts from 0 pore volume and ends at 20 pore volume while desorption started at 20 pore volume and ends at 50 pore volume.

3.2.3 Geochemical transport code PHREEQC

PHREEQC is a public domain geochemical package developed by the United States Geological Survey and is capable of calculating speciation, saturation-index as well as simulating batch-reaction, one-dimensional (1D) solute transport, reversible and irreversible reactions including aqueous, mineral, surface-complexation, ion-exchange equilibria, and other geochemical processes with a great diversity (Parkhurst and Appelo, 2013).

In the latest version 3, non-equilibrium reactions were added so dual-porosity can be modeled with stagnant zones incorporated in the column. Not only simple advective-reactive transport can be modeled, multicomponent diffusion (each solute diffuses corresponding to its own diffusion coefficient) can also be included using explicit finite-difference equations to define mixing among the stagnant cells.

Sorption and desorption processes can be characterized as surface complexation reactions, which can be described either by the CD-MUSIC (Charge Distribution MUltiSIte Complexation)

model or the model based on Dzombak and Morel (1990) database. The CD-MUSIC model allows multiple binding sites for each surface and the model based on Dzombak and Morel database is specialized for heavy metal ions on hydrous ferric oxide (ferrihydrite).

3.2.4 Procedure for using PHREEQC for modeling transport with sorption process

The model is established based on experiments described above. Surface complexation process for sorption and transport with stagnant zone (immobile zone) is simulated. Figure 3.4 shows the relationship between experimental procedure.

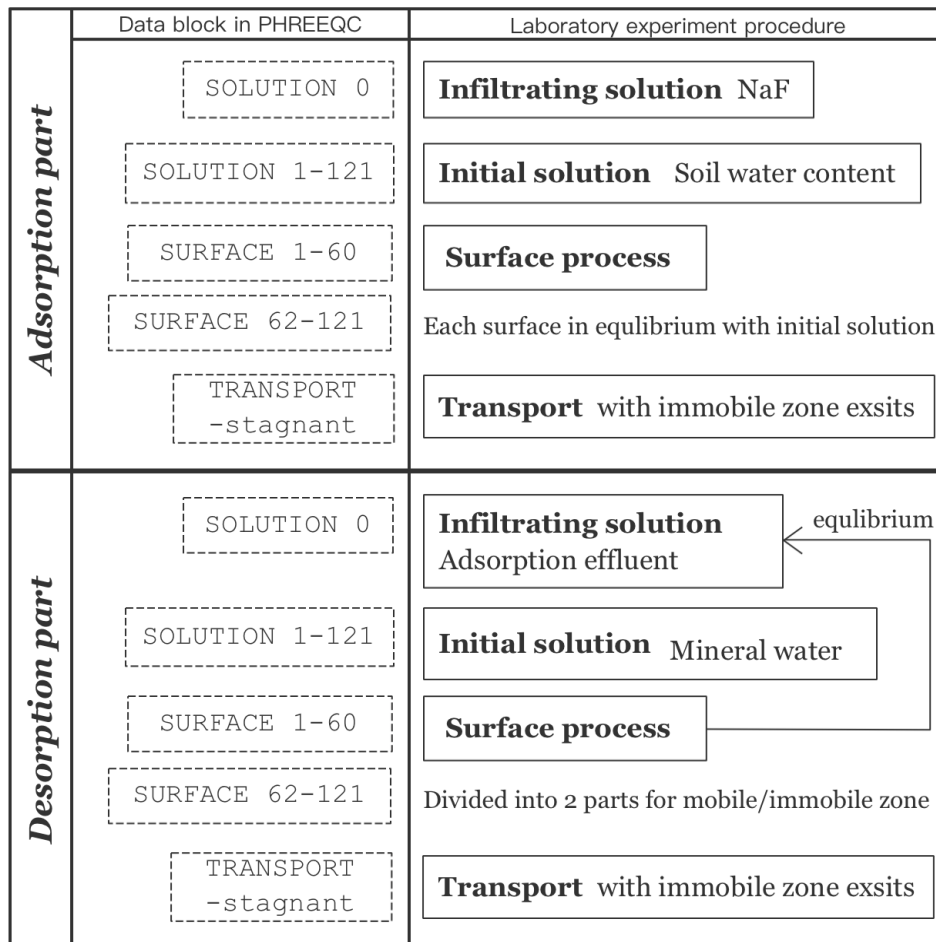


Figure 3.4 Logic of modeling using PHREEQC based on experiment procedures

1) Solution part:

In the SOLUTION part, chemical composition, temperature, pH, pe and pressure are defined for the initial solution and the infiltrating solution. The unit for solute concentration is mmol/kgw, where “mmol” indicates millimole and “/kgw” indicates per kilogram water. Usually, the infiltration solution will be defined as “SOLUTION 0” and “SOLUTION 1-*n*” is defined as the

initial solution for each cell, where the value of n is related to the cell numbers defined in the TRANSPORT part.

2) Surface part:

SURFACE defines the characteristics of each surface in a surface assemblage, such as the amount and composition. The composition can be defined both implicitly by assigning the surface assemblage in equilibrium with a solution of certain components or explicitly by defining the amounts of charge-balanced form surfaces. In this model, the implicit way is used, “SURFACE 1-60” and “SURFACE 62-121” are designated to equilibrate with solution 1 and solution 62 (the number will be discussed later in the transport part). Although multiple surfaces are defined, all of them can be in equilibrium with only one certain solution since all the compositions from “SOLUTION 1- n ” are identical.

The site unit in this model is defined as *density*. Two choices are optional, density and absolute. Absolute means the number of sites is given in moles; density means site density is used and site number is calculated from the site density and the surface area.

Three types of surfaces are available, namely diffuse double layer (DDL) surfaces, CD-MUSIC surfaces and non-electrostatic surfaces. In this model, DDL is chosen as the surfacer type.

3) Transport part:

TRANSPORT is the data block used to simulate 1D advection, advection-dispersion, diffusion and advection-dispersion with diffusive transport into stagnant zones. In PHREEQC, the scheme of transport models is unique to other hydrogeochemical transport models (Yeh and Tripathi, 1989). The equilibrium and chemical reactions are calculated twice: both after the advection and the dispersion step to minimize the numerical dispersion and iterations. Figure. 3.5 shows this unique scheme of the calculation process. Both after the advection and the dispersion step in order to minimize the numerical dispersion and iterations.

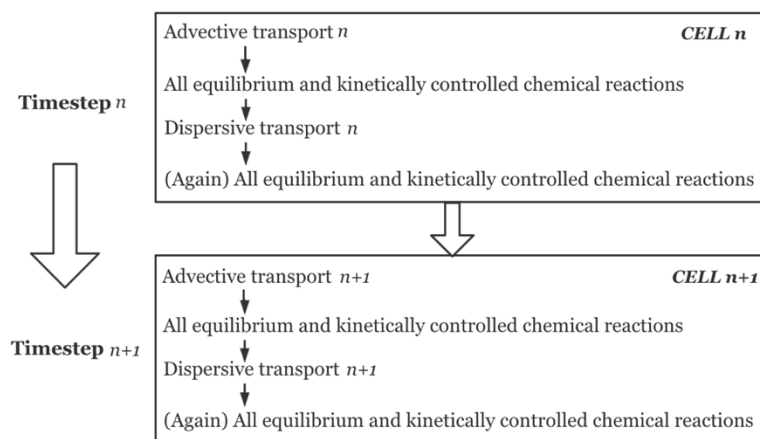


Figure 3.5 PHREEQC calculation process for transport modeling, drawn based on Parkhurst and Appelo (1999)

This approach increases the numerical accuracy and stability by adjusting the time step to grid size for each single part of the ADE equation. Numerical dispersion is minimized by controlling the relationship between time and distance discretization:

$$(\Delta t)_A \leq \frac{\Delta x}{v} \quad (3.8)$$

and numerical oscillations in diffusion and dispersions are eliminated by the restriction:

$$(\Delta t)_D \leq \frac{\Delta x^2}{3D_L} \quad (3.9)$$

Where $(\Delta t)_A$ is the time step for advective transport, $(\Delta t)_D$ the time step for diffusive and dispersive transport, Δx the cell length and D_L the hydrodynamic dispersion coefficient.

In many cases, numerical dispersion is negligible when $\Delta x \leq \alpha_L$. This means that the physical dispersion is of equal or even more importance with advection. But when the grid size is finer, i.e. cell length is smaller, $(\Delta t)_D$ is much smaller than $(\Delta t)_A$ due to the quadratic dependence. In order to solve this problem, multiple dispersion time step is added, $\sum (\Delta t)_D = (\Delta t)_A$. So in PHREEQC, the time step defined in the input file must be equal to the advection or diffusion time period. This is why an identifier “-shift” which indicates the number of $(\Delta t)_D$ or $(\Delta t)_A$ also must be defined in the calculation (Parkhurst and Appelo, 1999).

Flow direction is selected as forward, which means advective flow into higher numbered cells.

Also, the “correct_disp” is selected as true, indicating dispersivity is multiplied by $1 + \frac{1}{cells}$ for column end in order to improve effluent composition for flux boundary conditions.

The physical nonequilibrium process (in PHREEQC, the dual porosity model) is simulated by including the “-stagnant” identifier, which defines the maximum number of immobile cells adjacent to mobile cells, a first-order exchange factor that describes the diffusive mass transfer between mobile/immobile cells and porosity in each mobile/immobile cell and the maximum number of one mobile cell connected to immobile cell is assumed as 1 (“-stagnant_cells 1”).

It is worth mentioning that when including the “-stagnant” identifier, only defining “cell numbers” in the TRANSPORT keyword is not enough for modeling physical nonequilibrium processes. The concept of PHREEQC stagnant zone with reactions can be schemed as Figure. 3.6.

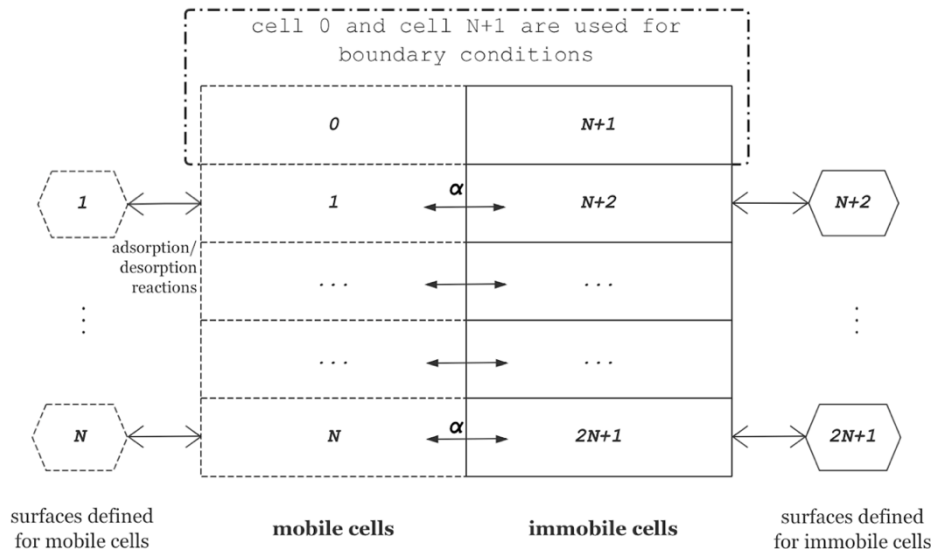


Figure 3.6 The concept of PHREEQC stagnant zone with reactions, drawn based on Parkhurst and Appelo (1999)

The “-cells” identifier refers only to the mobile cells, which means the immobile cells are defined separately. If cell 1 to N is defined for mobile cells, under the condition of “-stagnant” identifier, it means cell N+2 to cell 2N+1 is defined as immobile cells connecting the corresponding mobile zones. Cell 0 and N+1 is used for boundary conditions. So the infiltrating solution numbers should be defined from 1 to 2N+1, surfaces to be equilibrated with different kinds of cells are defined separately “1 to N” and “N+2 to 2N+1”. If not pay special attention to the numbering of SOLUTION and SURFACE, may lead to results that doesn’t include physical nonequilibrium process at all.

The flow rate variation is realized by adjusting the time step. Average pore velocity=cell length/time step. Flow rate thus calculated by substituting v into $Q = v\theta \cdot \pi r^2$. Where θ is total porosity and r is the radius of the soil column.

3.2.4 Validation of the numerical model

The simulation result of the advection-dispersion transport (equation 2.54) with sorption process was compared to the analytical solution used in PHREEQC (Ogata and banks,1961):

$$C = \frac{C_i}{2} \left(\operatorname{erfc} \left(\frac{1-x}{2\sqrt{\frac{x\alpha}{L}}} \right) + \exp \left(\frac{L}{\alpha} \right) \left(\operatorname{erfc} \left(\frac{1+x}{2\sqrt{\frac{x\alpha}{L}}} \right) \right) \right) \quad (3.10)$$

Where C is the concentration of effluent solution (mol/kgw), C_i the concentration of influent solution (mol/kgw), x the number of pore volume, α dispersivity (m) and column length L .

The boundary conditions are NaF solution with 50 mg/L fluoride at temperature 25 °C and pH=7, first type boundary condition at the first cell and third type boundary condition at last cell. Figure 3.7 shows the fit is relatively good but still with some discrepancies.

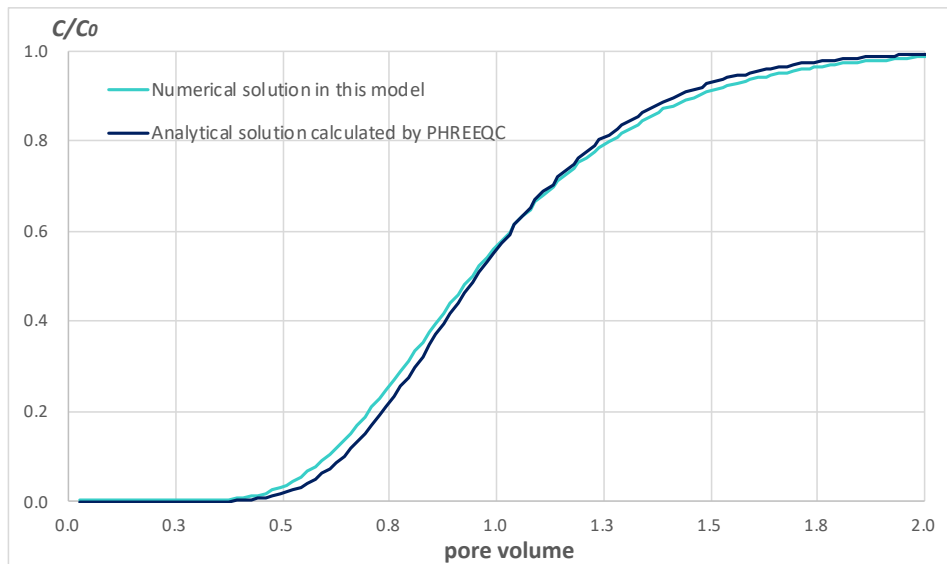


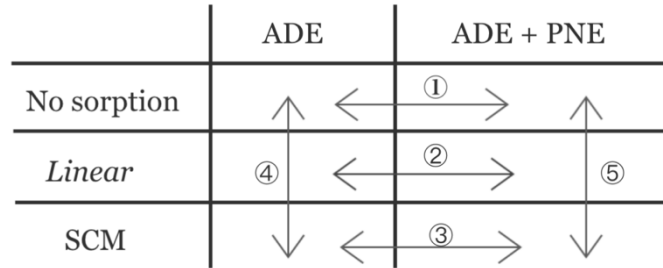
Figure 3.7 Comparison of the analytical solution and numerical result using.

IV. RESULTS

4.1 Simulation results

In this study, several numerical simulation cases were performed to discuss how transport under different flow rates and the different ratios of immobile zone in the total porosity contributes to fluoride transport and sorption processes in the modeled porous medium. The processes considered were, simple advection-dispersion (ADE) and advection-dispersion including physical nonequilibrium (PNE) processes for transport, and linear sorption (K_d) and surface complexation (SCM) models for sorption/desorption processes. Figure 4.1 shows the structure of the analysis how these processes impact the breakthrough curves.

Figure 4.1 The structure of the analysis for comparing different models in this study.



Three major cases were simulated, and these can be deviled into several subcases (details are shown in Appendix). For the simulation, the flow rate equal to the experimental case (3.4 ml/min) was selected, and the lowest flow rate (0.07 mL/min) was set based on the Peclet number to be 0.04, which was the condition that advection and diffusion played equally important roles in transport processes. Other flow rates were chosen for the convenience of calculation (e.g., 752mL/min, 376 mL/min...)

CASE I Impact of physical nonequilibrium transport and sorption processes on breakthrough curves.

① Impact of physical nonequilibrium transport on breakthrough curves (BTCs) at different flow rates under no sorption condition.

Simulation settings:

- Simple advection-dispersion transport process versus advection-dispersion transport process including physical nonequilibrium (flow rate to be 752mL/min);
- Simple advection-dispersion transport process versus advection-dispersion transport process including physical nonequilibrium (flow rate to be 0.07mL/min);

The results are shown in Figure 4.2:

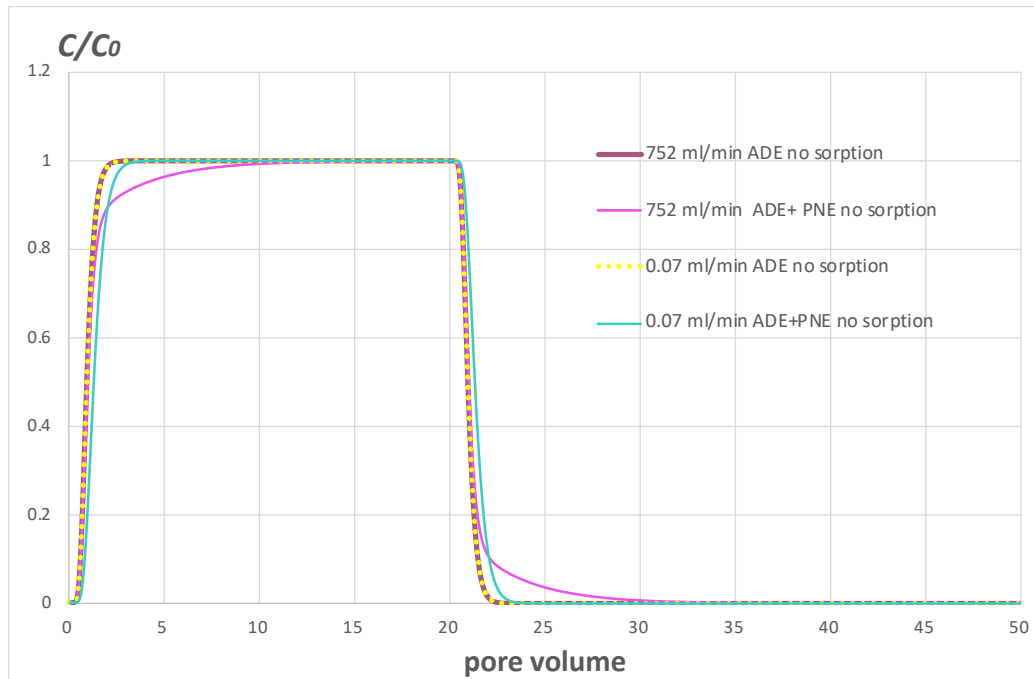


Figure 4.2 Relative concentrations of fluoride in the discharged solution as a function of pore volumes with different flow rates under no sorption condition. ADE indicates advection dispersion equation and PNE physical nonequilibrium process.

The peak concentrations were not much different at low flow rate, while at high flow rate, a decrease in peak concentration was observed until 12 pore volumes. When PNE was included, both high and low flow rates showed later breakthrough. An obvious tailing can be observed at high flow rate when PNE was included, but not obvious at low flow rate.

When flow rate was high and PNE was included, there existed insufficient time for the solute to transfer into the immobile zone by diffusion, so the concentration is lower than that of low flow rate at the same pore volume. The late breakthrough observed for both high and low flow rate conditions by including PNE was explained to be because solute transferred into immobile zones and solute concentration decreases.

② Impact of physical nonequilibrium transport process on breakthrough curves with linear sorption at different flow rates.

Simulation settings:

- Simple advection-dispersion transport process versus advection-dispersion transport process including physical nonequilibrium with linear sorption process (flow rate to be 752 mL/min);

- Simple advection-dispersion transport process versus advection-dispersion transport process including physical nonequilibrium with linear sorption process (flow rate to be 0.07 mL/min);

The results are shown in Figure 4.3:

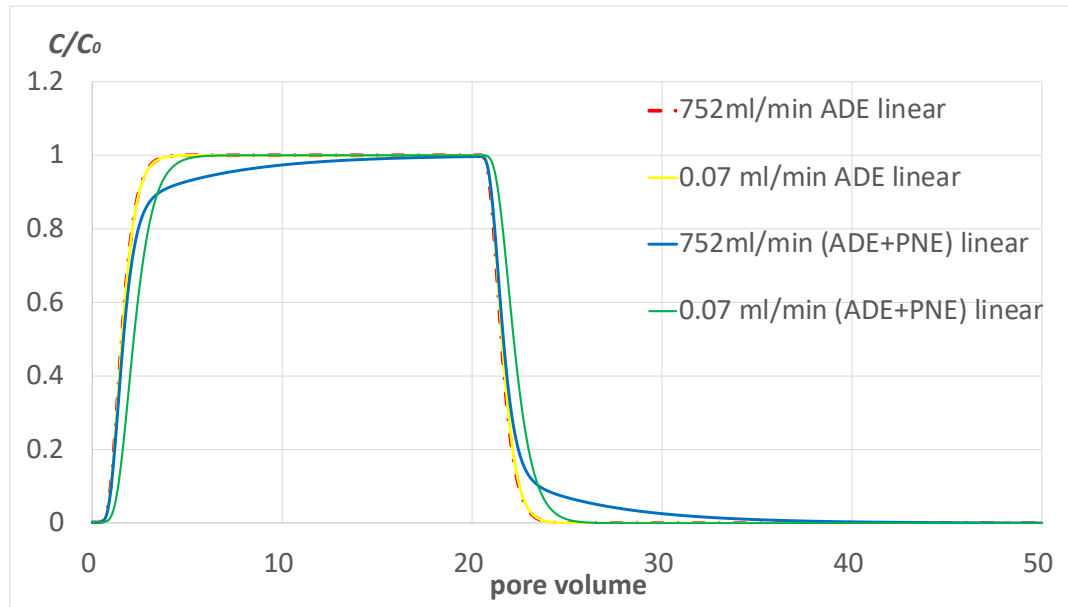


Figure 4.3 Relative concentrations of fluoride in the discharged solution as a function of pore volumes with different flow rates under linear sorption condition. ADE indicates advection dispersion equation and PNE physical nonequilibrium process.

When physical nonequilibrium transport process was added, the peak concentration decreased at high flow rate, while not in low flow rate. The tailing occurred at both flow rate but were more obvious at high flow rate. No matter PNE was added or not, high flow rate breakthrough earlier than low flow rate, because at the same pore volume, larger amount of solute was transported at higher flow rate.

③ Impact of physical nonequilibrium transport process on breakthrough curves with surface complexation model at different flow rates.

Simulation settings:

- Simple advection-dispersion transport process versus advection-dispersion transport process including physical nonequilibrium with surface complexation sorption model (flow rate to be 752 mL/min);
- Simple advection-dispersion transport process versus advection-dispersion transport process including physical nonequilibrium with surface complexation sorption model (flow rate to be 0.07 mL/min);

The results are shown in Figure 4.4:

When physical nonequilibrium transport process was included, the peak concentration decreased at high flow rate but not obvious at low flow rate. The later breakthrough was more obvious at low flow rate than that at high flow rate. Tailing was heavier at low flow rate due to sufficient resident time for sorption reactions than that at high flow rate.

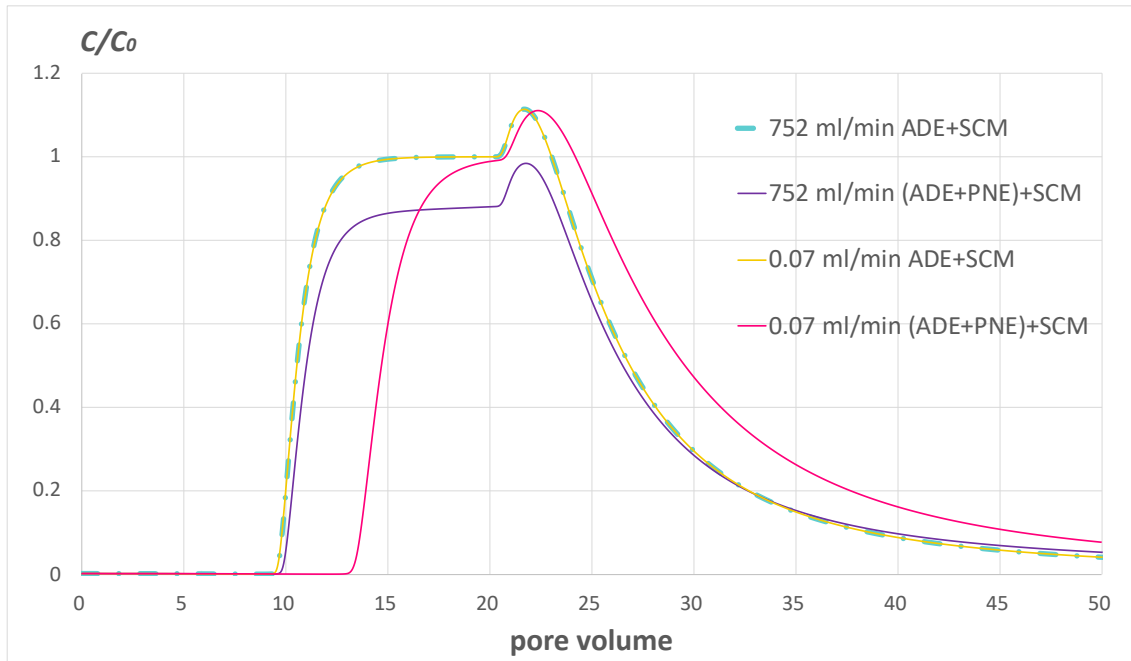


Figure 4.4 Relative concentrations of fluoride in the discharged solution as a function of pore volumes with different flow rates under surface complexation sorption model. ADE indicates advection dispersion equation, PNE physical nonequilibrium process and SCM surface complexation model.

④ Impact of sorption on breakthrough curves at different flow rates.

Simulation settings:

- No sorption versus linear sorption and surface complexation sorption model with simple advection-dispersion transport process (flow rate to be 752 mL/min);
- No sorption versus linear sorption and surface complexation sorption model with simple advection-dispersion transport process (flow rate to be 0.07 mL/min);

The results are shown in Figure 4.5:

When sorption was included, the breakthrough was later no matter which kind of sorption model was used compared to that with no sorption process. The BTCs using linear model at both flow rate breakthrough later than no-sorption BTCs but earlier than BTCs using surface complexation model. There was no difference between concentration peaks no matter sorption was included or not. Tailing exists when linear sorption model was used, but not very obvious compared to that when surface complexation model was included. The starting point was at 10

pore volumes when using surface complexation model, which seemed like have postponed compared to the linear model. Also, there was a distinct concentration peak (overshooting) when surface complexation model was used, which even exceeded the initial concentration.

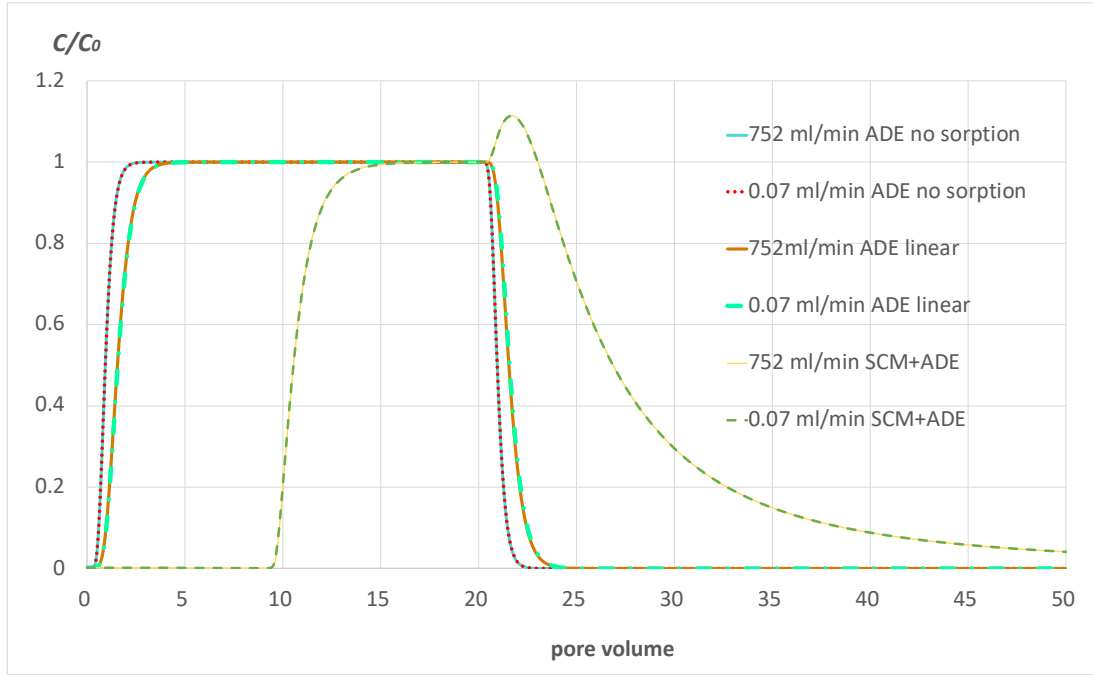


Figure 4.5 Relative concentrations of fluoride in the discharged solution as a function of pore volumes with different flow rates under no sorption, linear sorption condition and surface complexation model. ADE indicates advection dispersion equation and SCM surface complexation

The later breakthrough in both sorption model is due to solute adsorbed on sorption sites and two reasons may be used to explain why the different between using linear model and surface complexation model was so large. One is fluoride reactions with Al^{3+} and H^+ were included in the SCM (Equation 3.5 to 3.7) while not in the linear model (Equation 3.6), another may because PHRREQC is not very good at simulating linear sorption. It assumes a very large amount of surface sites, in this case, 1×10^{100} sites and this may not be the real case (Jaremalm *et al.*, 2013) and thus lead to some disabilities in linear sorption compared to its simulation on surface complexation models.

⑤ Impact of linear and surface complexation sorption processes on breakthrough curves with physical nonequilibrium transport at different flow rates.

Simulation settings:

- Simple advection-dispersion transport process versus advection-dispersion transport process including physical nonequilibrium with no sorption, linear and surface complexation sorption model (flow rate to be 752 mL/min);
- Simple advection-dispersion transport process versus advection-dispersion transport process including physical nonequilibrium with no sorption, linear and surface complexation sorption model (flow rate to be 0.07 mL/min);

The results are shown in Figure 4.6:

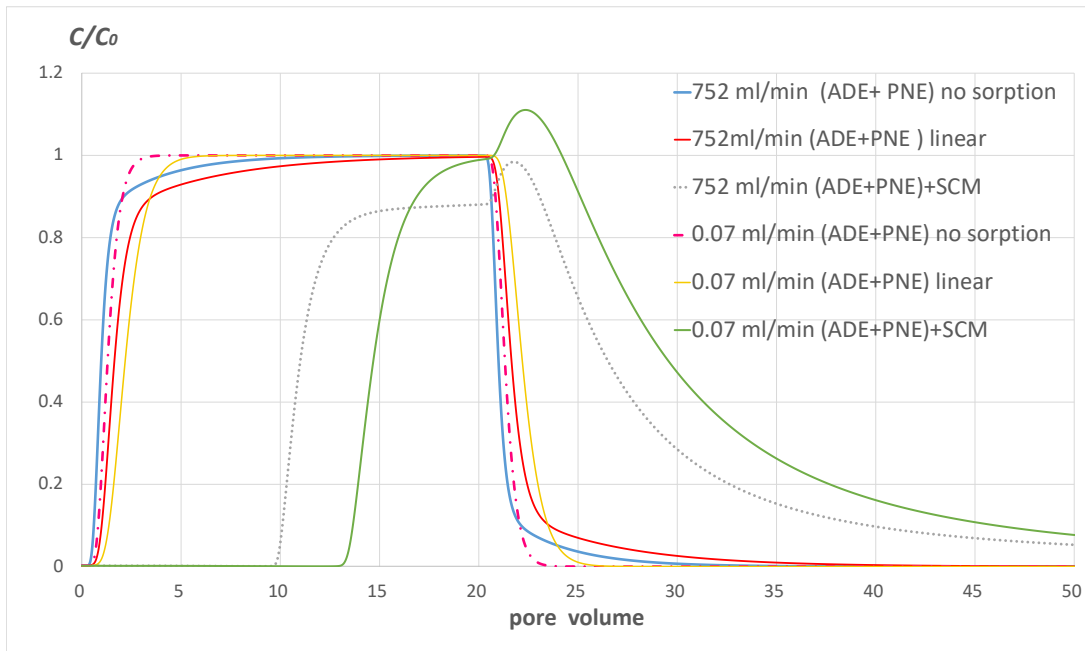


Figure 4.6 Relative concentrations of fluoride in the discharged solution as a function of pore volumes with different flow rates under no sorption, linear sorption condition and surface complexation model. ADE indicates advection dispersion equation, PNE physical nonequilibrium process and SCM surface complexation model

When transport process includes physical nonequilibrium, at low flow rate, the peak concentration was not changed as sorption was included, but at high flow rate, the peak largely decreased from 1 to 0.88. Tailings were more obvious when sorption was included and were heavier when surface complexation model was used. This is because fluoride that reacted with Al^{3+} and H^+ on the surface sites desorbed into water during desorption process. These reactions also lead to the delay in breakthrough when surface complexation model was used compared to linear model. The early breakthrough of all high flow rate than low flow rate at all sorption settings was because at the same pore volume, larger amount of solute was transported at higher flow rate. Overshooting occurred when surface process was included.

⑥ Impact of flow rate on breakthrough curves of mobile and immobile zones with physical nonequilibrium transport process and surface complexation model for sorption process.

Simulation settings:

- Advection-dispersion transport process including physical nonequilibrium with surface complexation sorption model at flow rate to be 752 mL/min versus 0.07 mL/min

The results are shown in Figure 4.7 and 4.8:

The breakthrough curves of immobile water are more of an analytical value rather than the real case because in reality, concentration of immobile water cannot be obtained by experiment. But analyzing this virtual BTCs gives us more information on the mass transfer between the mobile and immobile region.

At low flow rates, the concentration difference between mobile and immobile zone was smaller than that at high flow rate due to longer resident time. There was a time lag between mobile and immobile concentration increasing at high flow rate. This is because the majority of solute transported into immobile zone at high flow rate happens after the sorption started to equilibrate.

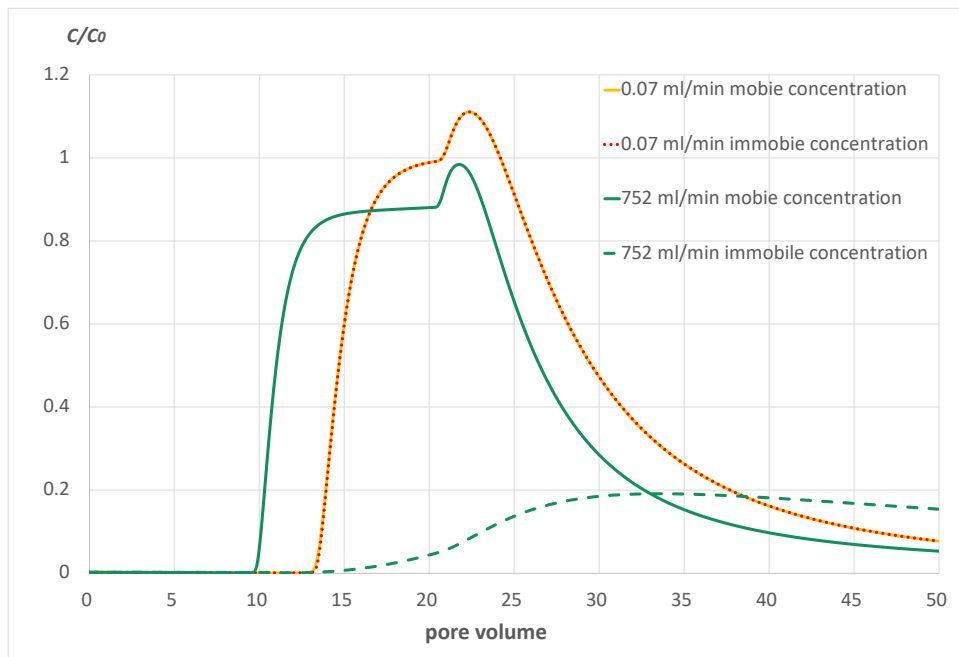


Figure 4.7 Relative concentrations of fluoride in the discharged solution as a function of pore volumes with different flow rates using surface complexation model. Mobile/immobile zone concentration at high/low flow rate till 50 pore volumes.

Although for the mobile zone, the residual concentration of low flow rate exceeded that of high flow rate, for a longer period (Figure 4.8), the immobile concentration surpassed the mobile concentration at low flow rate. This may indicate that during pumping of the drinking groundwater or remediation of fluoride contaminants, pumping too fast may not reach the desire goal but lead to large residual fluoride in soil.

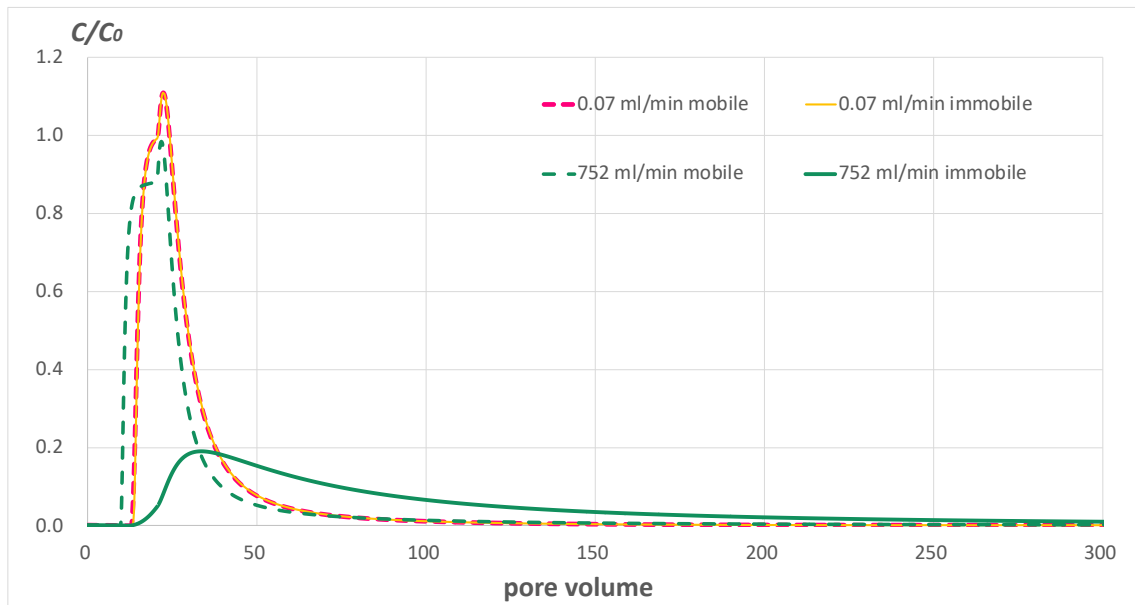


Figure 4.8 Relative concentrations of fluoride in the discharged solution as a function of pore volumes with different flow rates using surface complexation model. Mobile/immobile zone concentration at high/low flow rate till 300 pore volumes

CASE 2 Impact of flow rate on breakthrough curves of mobile and immobile zones with physical nonequilibrium transport process and surface complexation model for sorption process.

Simulation settings:

- Simple advection-dispersion transport process including physical nonequilibrium and surface complexation model for sorption at different flow rates (725 mL/min, 376 mL/min, 200 mL/min, 150 mL/min, 100 mL/min, 18 mL/min, 3.4 mL/min, 0.07 mL/min)

The results are shown in Figure 4.9 and 4.10:

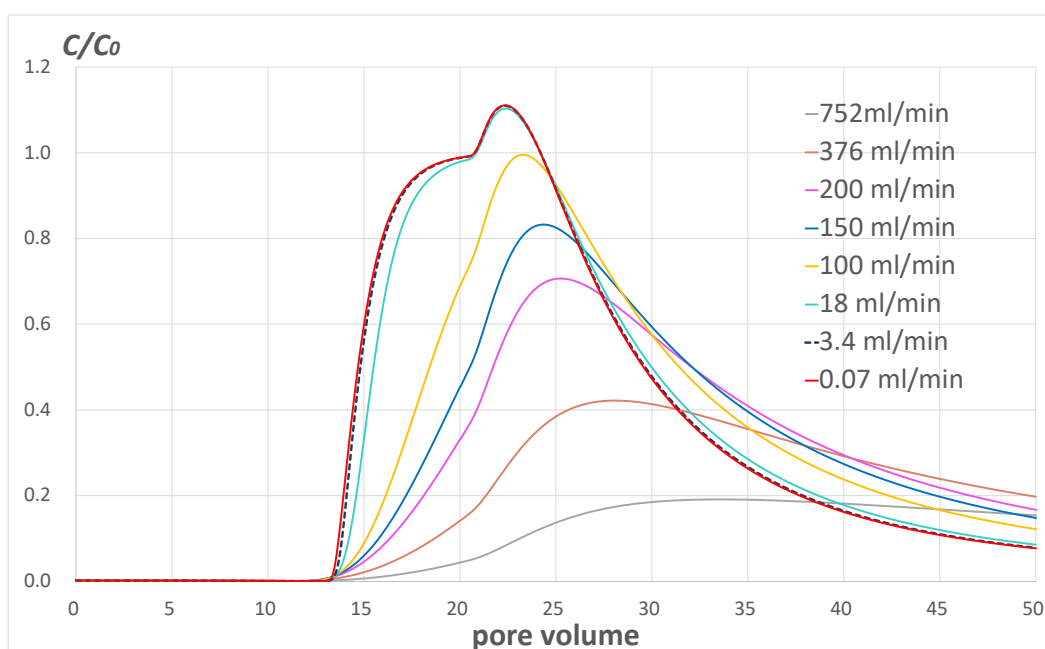


Figure 4.9 Relative concentrations of fluoride in the discharged solution as a function of pore volumes with different flow rates using surface complexation model.

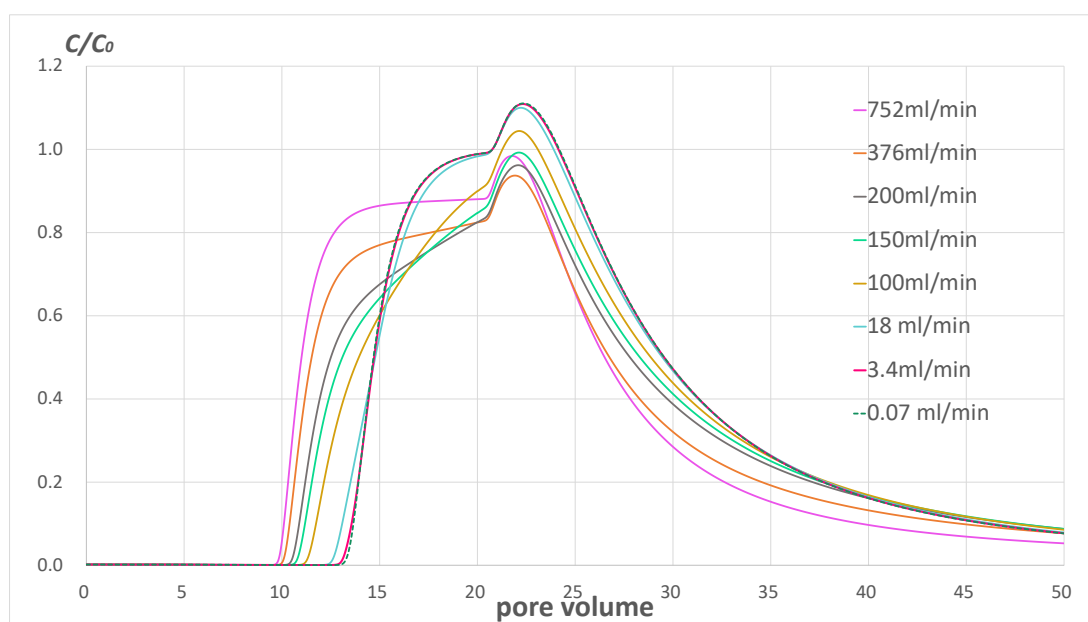


Figure 4.10 Relative concentrations of fluoride in the discharged solution as a function of pore volumes with different flow rates using surface complexation model.

As flow rate increased, the peak value of fluoride relative concentration decreased, and the frontal side of the breakthrough curve is left-shifted. Tailing was more obvious at lower flow rates. Till 50 pore volume, the concentrations of low flow rates were higher than those of high flow rates. A plateau is formed at relatively high concentration (376 and 752 mL/min).

The fluoride concentration in the immobile zone increases when flow rate decreased, the shape of breakthrough curve changed dramatically comparing to low flow rates when flow rate was high. The concentration when flow rate was 376 mL/min is the largest at 50 pore volumes. This may indicate that, at certain conditions, there existed an optimistic flow rate for solute transfer between mobile and immobile zones because the exchange factor was increasing to some extent with flow rate increasing (Bajracharya and Barry, 1997), however, if the flow rate is too high, there will be less time for the solute to enter the immobile zone.

CASE 3 Impact of immobile zone ratio on breakthrough curves of mobile and immobile zones with physical nonequilibrium transport process and surface complexation model for sorption process.

① Impact of immobile zone ratio on breakthrough curves of mobile and immobile zones at high and low flow rate.

Simulation settings:

- Simple advection-dispersion transport process including physical nonequilibrium and surface complexation model for sorption at immobile zone ratios (0.3, 0.5, 0.7)

The results are shown in Figure 4.10 and 4.11:

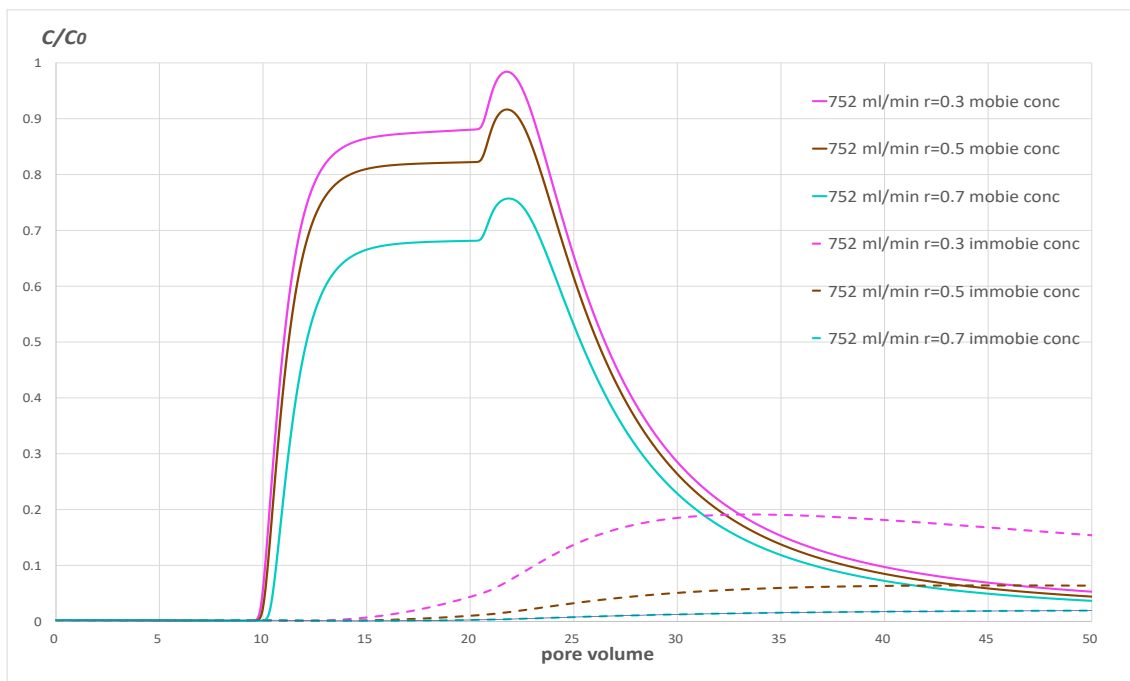


Figure 4.10 Relative concentrations of fluoride in the discharged solution as a function of pore volumes with different flow rates using surface complexation model. r

indicating immobile zone ratio

With the increase of ratio of immobile zone, the maximum relative solute concentration in the mobile zone decreased from 0.88 to 0.68 ($r=0.3$ to $r=0.7$, respectively) and until 50 pore volumes, the maximum relative solute concentration in the immobile zone also decreased from 0.19 to 0.01 ($r=0.3$ to $r=0.7$, respectively). Although the flow rate was high, if the area for mass transfer increased, the solute loss from bulk solution into the immobile zones will increase, which resulted in a drop in maximum relative concentration if immobile ratio increased from 0.3 to 0.7. For the immobile zone concentrations, $r = 0.7$ was about 9 times smaller than that of $r = 0.3$ at 30 pore volumes. This is because more solute was adsorbed on to the sites in the immobile zone when r was high, so the concentration in the fluid was lower.

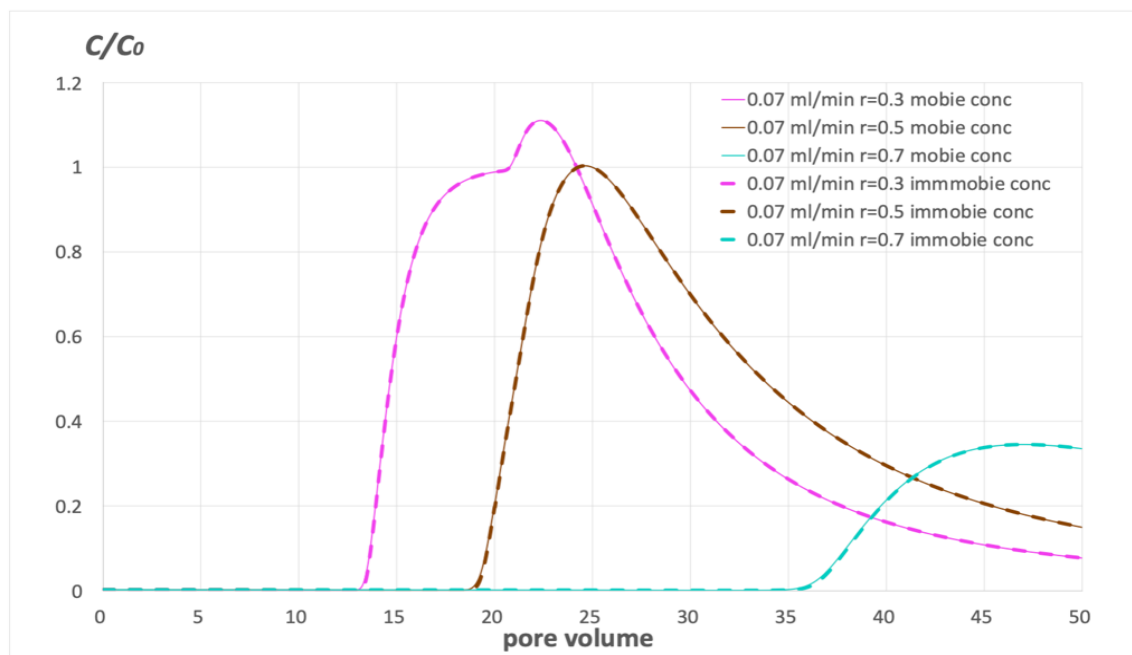


Figure 4.11 Relative concentrations of fluoride in the discharged solution as a function of pore volumes with different flow rates using surface complexation model. r indicating immobile zone ratio

The increase of the ratio of immobile zone from 0.3 to 0.5 resulted in small changes in maximum relative solute concentration in both mobile and immobile zones. But when the ratio increased to 0.7, the concentration in both zones decreased dramatically from 0.99 to 0.10 ($r = 0.3$ to $r = 0.7$)

② Impact of immobile zone ratio on breakthrough curves of mobile and immobile zones at different flow rates.

Simulation settings:

- Simple Advection-dispersion transport process including physical nonequilibrium and surface complexation model for sorption at different flow rates (725 mL/min, 376 mL/min, 18 mL/min, 3.4 mL/min, 0.07 mL/min) with different immobile zone ratio ($r = 0.3, 0.5, 0.7$)

Results are shown in Figure 4.12.

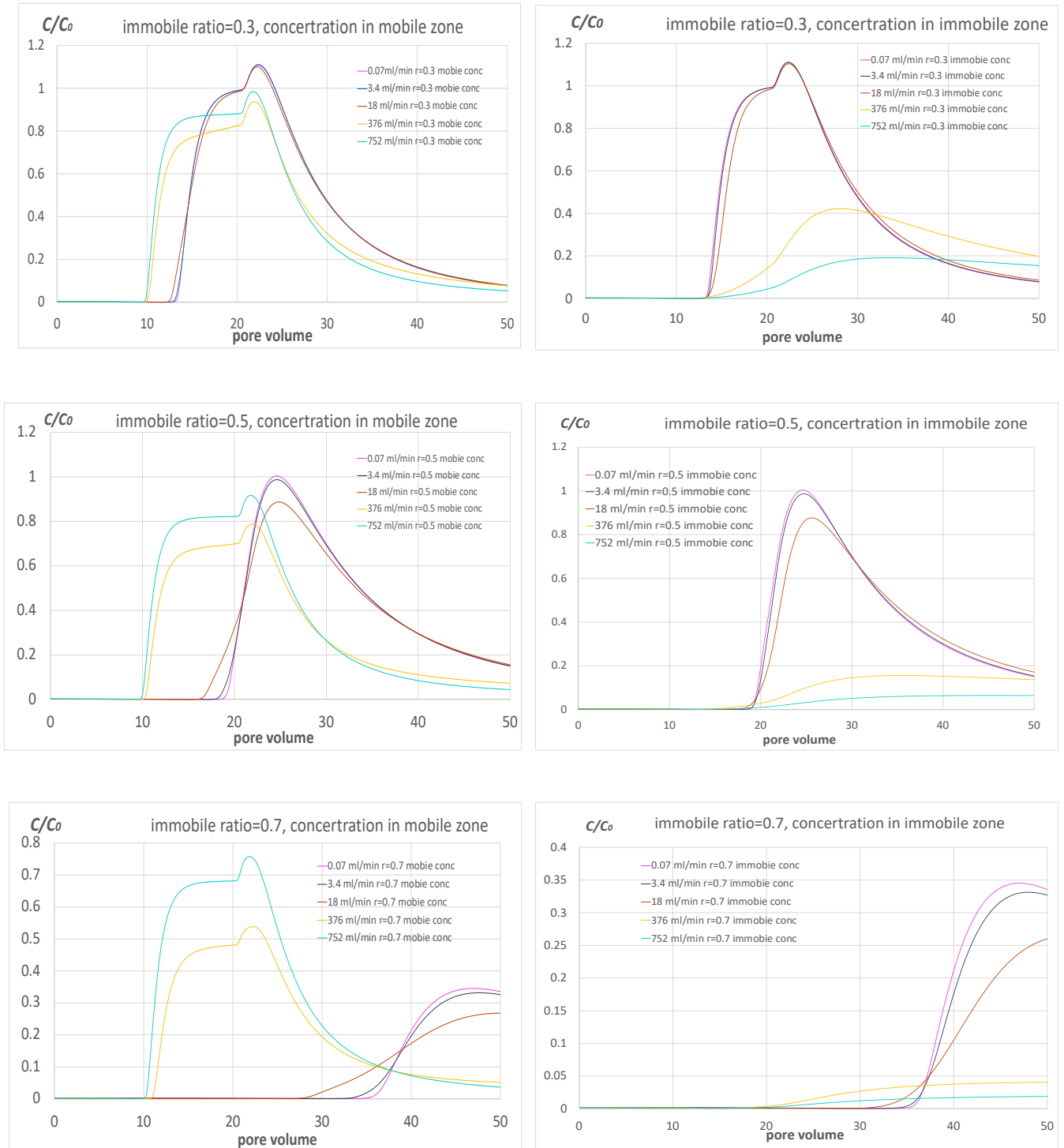


Figure 4.12 Relative concentrations of fluoride in the discharged solution as a function of pore volumes with different flow rates using surface complexation model. r indicating immobile zone ratio

With the increase of immobile zone ratio, the starting point of mobile concentration BTCs postponed largely than that at higher flow rate. The reason this happened is that, before the sorption equilibrated, although the immobile zone ratio was larger, the velocity was high enough to transmit the same amount of solute at a relatively same time.

With the ratio of immobile zone increasing, the shape of BTCs at lower flow rates changed remarkably than those of higher flow rates. When the ratio = 0.7, the desorption half of the BTCs were not observable within 50 pore volumes. This is because that when the immobile area was larger, there will be more mass being transferred into it, and since in this model, equal amount of sorption sites was defined for both mobile and immobile zone, there will be more solute adsorbed onto the sites inside immobile zones. So, the kickoff of BTCs at lower flow rate was later.

CASE 4 Immobile concentration distribution in the flow direction.

Simulation settings:

- Simple advection-dispersion transport process including physical nonequilibrium and surface complexation model for sorption at different flow rates (725 mL/min and 0.07 mL/min)

The results are shown in Figure 4.13 and 4.14.

Cell 1 and cell 60 were the first and last cell of the mobile zone, and cell 62 and 121 were the first and last cell of the immobile zone, respectively.

As the solute transported from the first cell to the last cell, the kickoff point of concentration started from zero was later and the overshooting was more obvious.

At low flow rate, there is only scarcely different between the mobile and immobile concentration along the flow direction, while at high flow rate, the difference is obvious: the shape of BTC changes dramatically and the peak of relative concentration reduces from 1.0 to 0.88 in the mobile zone and 0.3 to 0.19 in the immobile zone. This is because when the exchange factor is fixed, the total mass that is transfer from the mobile zone into the immobile zone by diffusion is also fixed, but when the flow rate is high, the solute being transported in the mobile zone by advection is increased, so the concentration difference is more obvious at high flow rate.

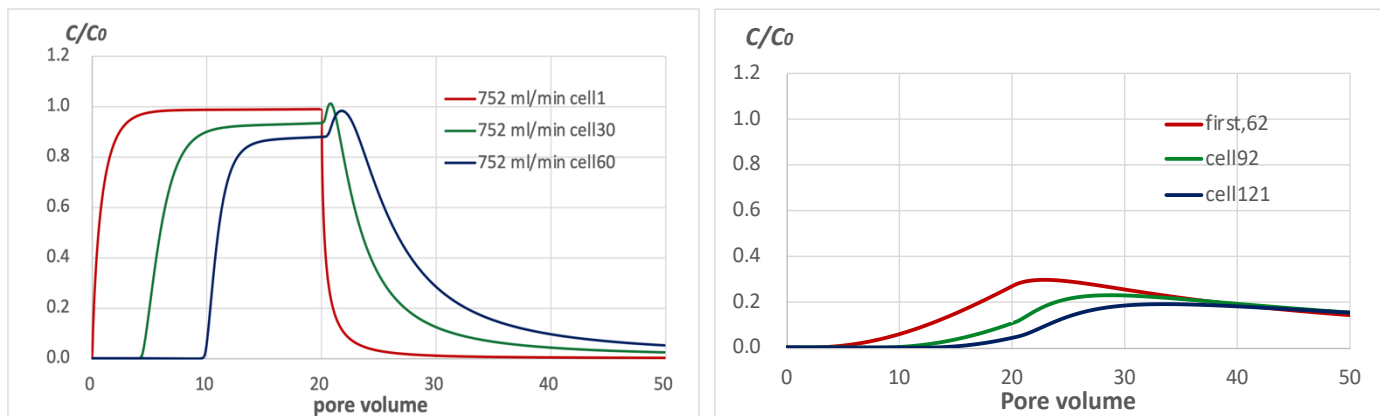


Figure 4.13 Relative concentration of fluoride in the mobile/immobile zones versus time at high flow rate at different part of the soil column

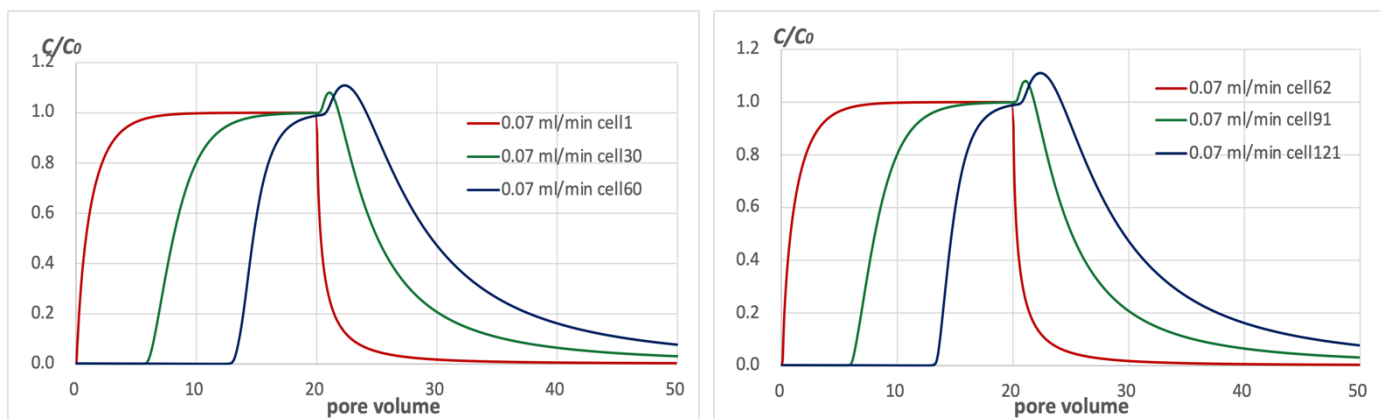


Figure 4.14 Relative concentration of fluoride in the mobile/immobile zones versus time at low flow rate at different part of the soil column

V. DISCUSSIONS

5.1 Comparison between the model and the experimental data

Parameter used in this model, same as in experiments by Padhi (2015),

Table 5.1 Parameters used for the fitting with experimental data

Parameter	Value	Unit
Total porosity	0.39	
Mass transfer coefficient	1.32×10^{-3}	s^{-1}
Mobile water fraction	0.76	

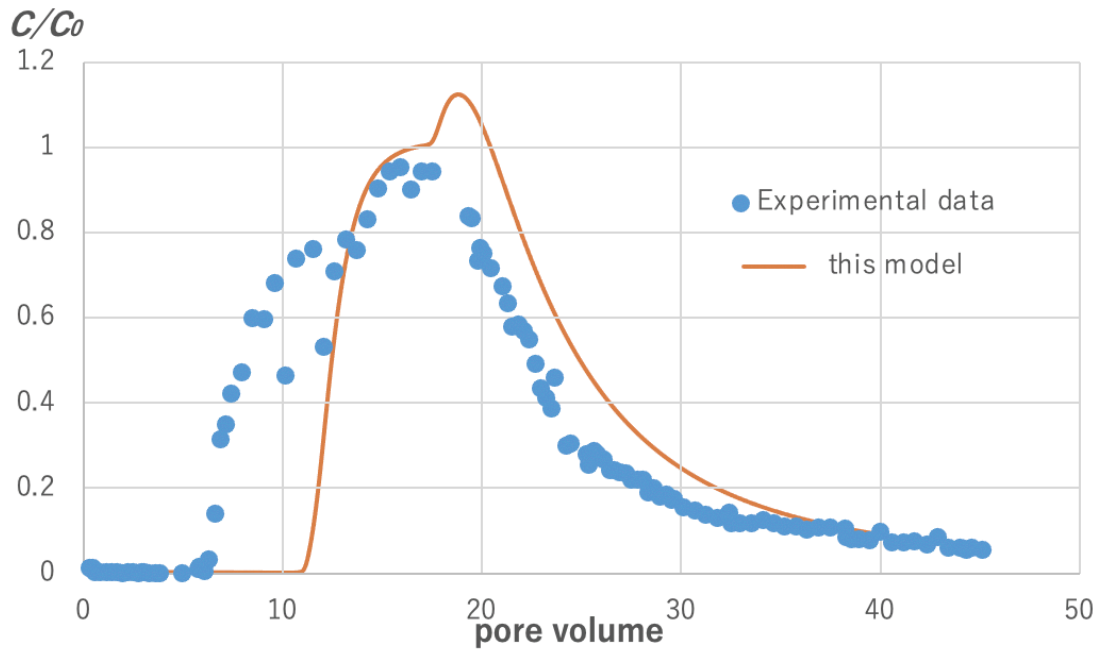


Figure 5.1 A comparison between the model and the experimental data.

This model provides a relatively good fit to the desorption part of the BTC, but poorly on the adsorption part. The tailing is also well predicted but still cannot explain what happened in the experimental data at about 13 pore volume. In order to obtain a better fitting, several modified cases are simulated.

5.2 Modified cases

1) Changing the magnitude of the exchange factor α .

The exchange factor α used is 1.32×10^{-3} , which was estimated from experiment.

Simulation settings:

- Advection-dispersion transport process including physical nonequilibrium and surface complexation model for sorption with different exchange factor α (1.32×10^{-10} , 1.32×10^{-3} , 1.32×10^2 , 1.32×10^5), at a flow rate of 3.4 mL/min.

Results are shown in Figure 5.1.

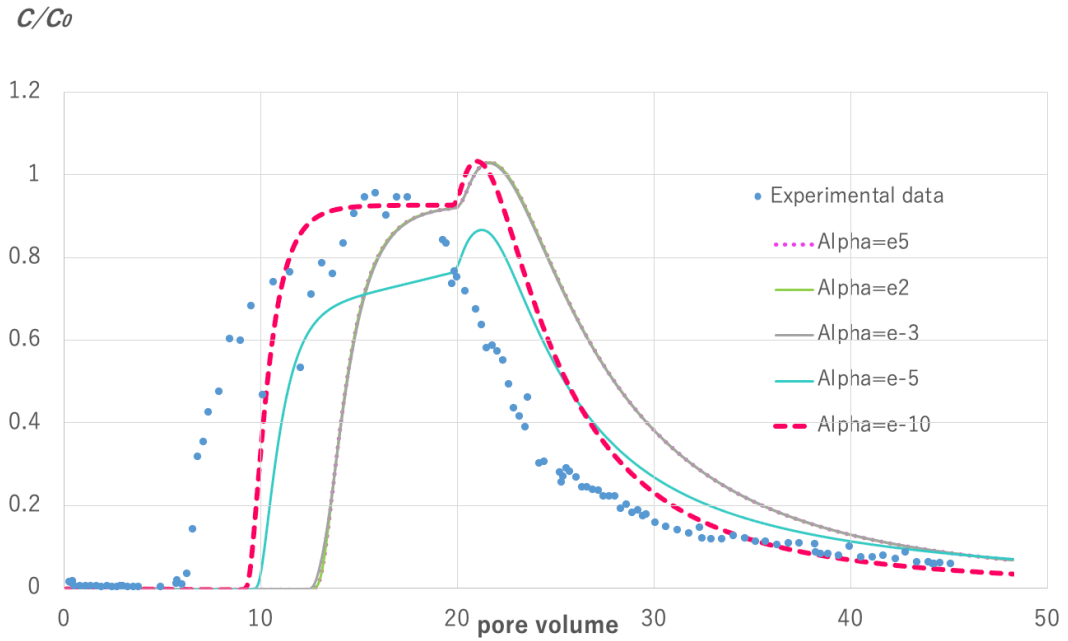


Figure 5.2 Fluoride relative concentration versus pore volume at different magnitude of the exchange factor α

From figure 5.1, we can know that this value is considered large for the difference between $\alpha = e^{-10}$ (10^{-10}) and $\alpha = e^{-3}$ (10^{-3}) is very small. According to PHRQEEC manual version2 (Parkhurst and Appelo, 1999), α can be calculated by:

$$\alpha = \frac{D_e \theta_{im}}{(a f_{s \rightarrow 1})^2} \quad (5.1)$$

Where D_e is the molecular diffusion coefficient (m^2/s), θ_{im} is the porosity for immobile zone, a the average diameter of particles (m) and $f_{s \rightarrow 1}$ is a shape factor for first-order -model conversion.

For the NaF concentration, De at 25°C is about $1.37 \times 10^{-9} \text{ m}^2/\text{s}$ (Ribeiro *et al.*, 2010), $\theta_{im}=0.111$, $a=0.006$ and $f_{s \rightarrow 1}=0.21$ for sphere. These values result to an alpha at a magnitude of e^{-5} , which seems to fit the data better than the origin α estimated.

From chapter 4, we know that the higher the immobile ratio in total porosity, the later the BTC starts from zero at low flow rates. So, another moderate by increasing this ration was simulated.

2) Changing the immobile zone ratio.

Simulation settings:

- Advection-dispersion transport process including physical nonequilibrium and surface complexation model for sorption with the immobile zone ratio equals 0.15, at a flow rate of 3.4 mL/min.

Result is shown in Figure 5.2.

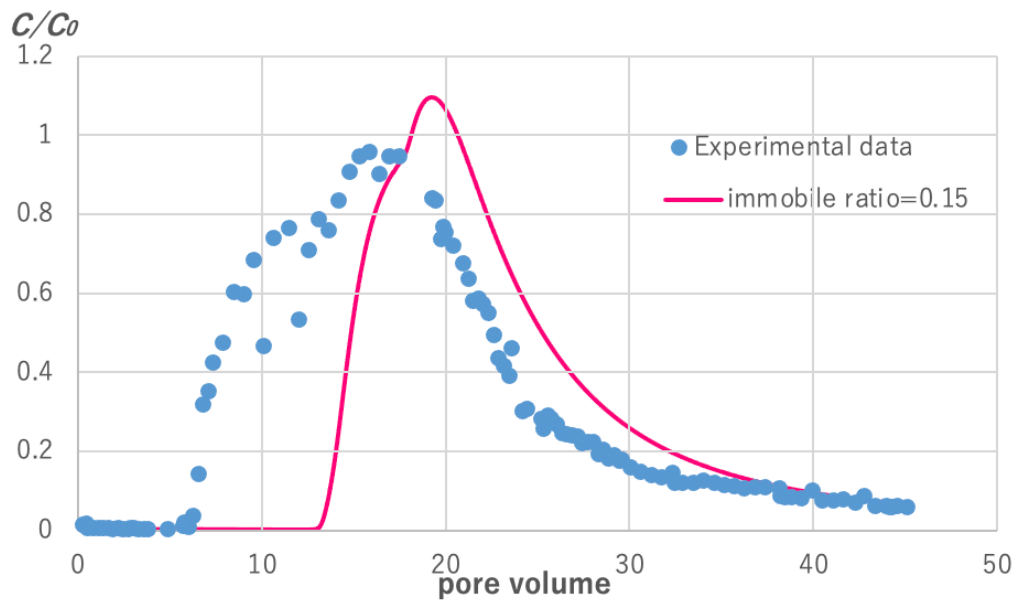


Figure 5.3 Experimental data fitting with immobile ratio=0.15.

As shown in Figure 5.2. The fitting does not improve much, so another case is simulated using exchange factor $\alpha=1.32 \times 10^{-5}$ and immobile ratio equals to 0.15.

3) Changing the exchange factor and immobile ratio

Simulation settings:

- Advection-dispersion transport process including physical nonequilibrium and surface complexation model for sorption with the exchange factor $\alpha=1.32 \times 10^{-5}$ and immobile ratio equals to 0.15, at a flow rate of 3.4 mL/min.

Result is shown in Figure 5.3.

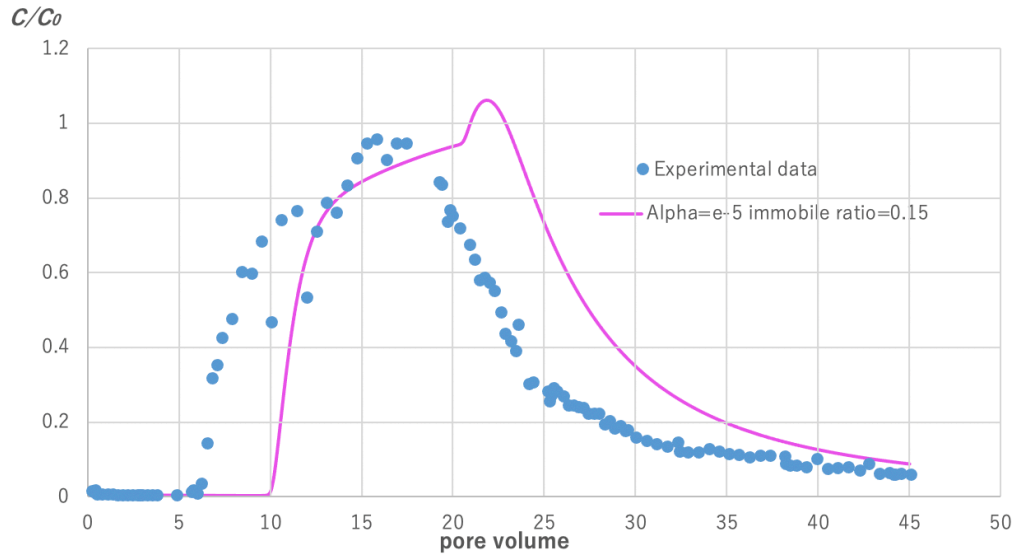


Figure 5.4 Experimental data fitting with exchange factor $\alpha=1.32 \times 10^{-5}$ and immobile ratio equals to 0.15.

As shown in Figure 5.3, model using these parameters results in a better fitting in the peak value of the concentration and desorption part of the BTC, but still cannot fit the pore volume when the concentration increases from zero. This may because a smaller exchange factor or a larger immobile zone ratio is used.

VI. CONCLUSION

6.1 Summary

Fluoride is beneficial for preventing dental caries and skeleton strength if consumed properly but can also lead to disease such as skeletal fluorosis if the intake exceeds the recommended level. In many parts of the world, especially rural areas in developing countries people depend on groundwater as drinking water, if the climate is semi-arid or arid, there is a great possibility that the fluoride concentration in the water exceeds the general limitation. In these areas, the removal of fluoride is realized by first pumping out then either adsorbed by absorbent or from sediment by adding chemicals. During pumping, there is a chance for deep, old high-fluoride groundwater to contaminate shallow groundwater. Also, in contaminant remediation procedure, “pump and treat” is a common way to remove fluoride from soil. The efficiency of these methods using pumps can be affected by pumping rate, higher pumping rate means higher flow rate in the soil.

In order to understand how fluoride sorption behavior is impacted by flow rate, a fluoride transport model with sorption process was built, and numerical simulations with different flow rates were conducted. Also, how physical nonequilibrium transport and sorption process contribute to fluoride behavior in soil is simulated.

The main result obtained from the simulations were as follows.

For different flow rates, when transport is explained by advection-dispersion equation with immobile zone, and surface complexation processes used for sorption process, when flow rate is low, the solute concentration difference between the mobile and immobile zone is small because the resident time is long and the mass transfer is more sufficient. When flow rate is high, there is an obvious time lag and concentration difference between the mobile and immobile zones because the resident time is short for mass to transfer as soon as contacting the immobile zone.

The increase of immobile zone ratio impacts greater on fluoride concentrations at low flow rates because more immobile zone means more important role diffusion plays.

The comparison of model results and experimental data showed that the surface complexation model explains fluoride behavior better than linear K_d model.

6.2 Implications

The results of this study show that high flow rate may lead to a higher residual fluoride concentration in the fraction of water that solute can only be transported in by diffusion (immobile water), which can be applied during pumping high-fluoride concentration groundwater. The

pumping rate should not be too high in order to avoid the solute in the immobile zones diffuse back in to the low-fluoride concentration water.

When the immobile zone in the soil occupies a higher ratio in total porosity, the pump rate should be higher since the ratio impacts less on concentration at higher flow rates.

6.3 Future work and recommendations

- 1) Modification cases with a larger exchange factor or a smaller immobile zone ratio should be simulated to improve the fitting with experimental data;
- 2) Experiment should be done to check the fitting at higher flow rates with flow interruption;
- 3) Flow interruption should be started at a relative concentration over 0.8 for a longer period and to confirm the existence of physical nonequilibrium;

APPENDIX

Case No.	Flow rate (mL/min)	Immobile zone ratio	Sorption process	Transport process	Exchange factor α (s ⁻¹)
1	0.07	0.3	—	ADE	$1.32 \times e^{-3}$
2	0.07	0.3	—	PNE	$1.32 \times e^{-3}$
3	0.07	0.3	Linear K_d	ADE	$1.32 \times e^{-3}$
4	0.07	0.3	Linear K_d	PNE	$1.32 \times e^{-3}$
5	0.07	0.3	SCM	ADE	$1.32 \times e^{-3}$
6	0.07	0.3	SCM	PNE	$1.32 \times e^{-3}$
7	0.07	0.5	SCM	PNE	$1.32 \times e^{-3}$
8	0.07	0.7	SCM	PNE	$1.32 \times e^{-3}$
9	3.4	0.3	SCM	PNE	$1.32 \times e^{-3}$
10	3.4	0.5	SCM	PNE	$1.32 \times e^{-3}$
11	3.4	0.7	SCM	PNE	$1.32 \times e^{-3}$
12	3.4	0.3	SCM	PNE	$1.32 \times e^5$
13	3.4	0.3	SCM	PNE	$1.32 \times e^2$
14	3.4	0.3	SCM	PNE	$1.32 \times e^{-5}$
15	3.4	0.3	SCM	PNE	$1.32 \times e^{-10}$
16	18	0.3	SCM	PNE	$1.32 \times e^{-3}$
17	18	0.5	SCM	PNE	$1.32 \times e^{-3}$
18	18	0.7	SCM	PNE	$1.32 \times e^{-3}$
19	376	0.3	SCM	PNE	$1.32 \times e^{-3}$
20	376	0.5	SCM	PNE	$1.32 \times e^{-3}$
21	376	0.7	SCM	PNE	$1.32 \times e^{-3}$
22	752	0.3	—	ADE	$1.32 \times e^{-3}$
23	752	0.3	—	PNE	$1.32 \times e^{-3}$
24	752	0.3	Linear K_d	ADE	$1.32 \times e^{-3}$
25	752	0.3	Linear K_d	PNE	$1.32 \times e^{-3}$
26	752	0.3	SCM	ADE	$1.32 \times e^{-3}$
27	752	0.3	SCM	PNE	$1.32 \times e^{-3}$
28	752	0.5	SCM	PNE	$1.32 \times e^{-3}$
29	752	0.7	SCM	PNE	$1.32 \times e^{-3}$

REFERENCES

- Aoba, T. (1997). The effect of fluoride on apatite structure and growth. *Critical Reviews in Oral Biology & Medicine*, 8(2), 136-153.
- Appelo, C. A. J., & Postma, D. (2004). *Geochemistry, groundwater and pollution*. CRC press.
- Bajracharya, K., & Barry, D. A. (1997). Nonequilibrium solute transport parameters and their physical significance: Numerical and experimental results. *Journal of contaminant hydrology*, 24(3-4), 185-204.
- Bear, J., Nichols, E., Kulshrestha, A., & Ziagos, J. (1994). Effect of contaminant diffusion into and out of low-permeability zones (No. UCRL-ID-115626). Lawrence Livermore National Lab., CA (United States).
- Bernstein, D. S., Sadowsky, N., Hegsted, D. M., Guri, C. D., & Stare, F. J. (1966). Prevalence of osteoporosis in high-and low-fluoride areas in North Dakota. *JAMA*, 198(5), 499-504.
- Bethke, C. M., & Brady, P. V. (2000). How the Kd approach undermines ground water cleanup. *Groundwater*, 38(3), 435-443.
- Brusseau, M. L., & Rao, P. S. C. (1990). Modeling solute transport in structured soils: A review. *Geoderma*, 46(1-3), 169-192.
- Brusseau, M. L., Hu, Q., & Srivastava, R. (1997). Using flow interruption to identify factors causing nonideal contaminant transport. *Journal of Contaminant Hydrology*, 24(3-4), 205-219.
- Brusseau, M. L., Rao, P. S. C., Jessup, R. E., & Davidson, J. M. (1989). Flow interruption: A method for investigating sorption nonequilibrium. *Journal of Contaminant Hydrology*, 4(3), 223-240.
- Cerklewski, F. L. (1997). Fluoride bioavailability—nutritional and clinical aspects. *Nutrition research*, 17(5), 907-929.
- Chapman, S. W., & Parker, B. L. (2005). Plume persistence due to aquitard back diffusion following dense nonaqueous phase liquid source removal or isolation. *Water Resources Research*, 41(12).
- Chikte, U. M., Louw, A. J., & Stander, I. (2001). Perceptions of fluorosis in northern Cape communities. *SADJ: journal of the South African Dental Association= tydskrif van die Suid-Afrikaanse Tandheelkundige Vereniging*, 56(11), 528.
- Chow, L. C. (1990). Tooth-bound fluoride and dental caries. *Journal of dental research*, 69(2_suppl), 595-600.
- Chowdhury, A., Adak, M. K., Mukherjee, A., Dhak, P., Khatun, J., & Dhak, D. (2019). A critical review on geochemical and geological aspects of fluoride belts, fluorosis and natural materials and other sources for alternatives to fluoride exposure. *Journal of Hydrology*, 574, 333-359.
- Cronin, S. J., Manoharan, V., Hedley, M. J., & Loganathan, P. (2000). Fluoride: A review of its

fate, bioavailability, and risks of fluorosis in grazed-pasture systems in New Zealand. *New Zealand Journal of Agricultural Research*, 43(3), 295-321.

Dahi, E. (1996, September). Contact precipitation for defluoridation of water [Discussion paper]. In *Reaching the unreached-Challenges for the 21st century: Proceedings of the 22nd WEDC International Conference*, New Delhi, India (pp. 262-265). cc WEDC, Loughborough University.

De Smedt, F., & Wierenga, P. J. (1979). Mass transfer in porous media with immobile water. *Journal of hydrology*, 41(1-2), 59-67..

Deans, H. A. (1963). A mathematical model for dispersion in the direction of flow in porous media. *Society of Petroleum Engineers Journal*, 3(01), 49-52.

Dzombak, D. A., & Morel, F. M. (1990). *Surface complexation modeling: hydrous ferric oxide*. John Wiley & Sons.

Edition, F. (2011). Guidelines for drinking-water quality. *WHO chronicle*, 38(4), 104-8.

Edmunds, W. M., & Smedley, P. L. (2013). Fluoride in natural waters. In *Essentials of medical geology* (pp. 311-336). Springer, Dordrecht.

Fawell, J., Bailey, K., Chilton, J., Dahi, E., & Magara, Y. (2006). *Fluoride in drinking-water*. IWA publishing.

Fesch, C., Simon, W., Haderlein, S. B., Reichert, P., & Schwarzenbach, R. P. (1998). Nonlinear sorption and nonequilibrium solute transport in aggregated porous media: Experiments, process identification and modeling. *Journal of Contaminant Hydrology*, 31(3-4), 373-407

Fetter, C. W., Boving, T. B., & Kremer, D. K. (1999). *Contaminant hydrogeology* (Vol. 500). Upper Saddle River, NJ: Prentice hall.

Freeze, R. A., & Cherry, J. A. (1979). *Groundwater*. Englewood Cliffs, N.J: Prentice-Hall.

Fuge, R., & Andrews, M. J. (1988). Fluorine in the UK environment. *Environmental Geochemistry and Health*, 10(3-4), 96-104.

Gilbert, O., Hernández, M., Vilanova, E., & Cornella, O. (2014). Guideline protocol for soil-column experiments assessing fate and transport of trace organics. Demeau, European Union: Brussels, Belgium.

Goldberg, S. (1992). Use of surface complexation models in soil chemical systems. In *Advances in agronomy* (Vol. 47, pp. 233-329). Academic Press.

Goldberg, S., Criscenti, L. J., Turner, D. R., Davis, J. A., & Cantrell, K. J. (2007). Adsorption-desorption processes in subsurface reactive transport modeling. *Vadose Zone Journal*, 6(3), 407-435.

HOHL, H., SIGG, L., & STUMM, W. (1980). Characterization of surface chemical properties of oxides in natural waters: the role of specific adsorption in determining the surface charge.

Healy, W. B., & Drew, K. R. (1970). Ingestion of soil by hoggets grazing swedes. *New Zealand*

journal of agricultural research, 13(4), 940-944

Hem, J. D. (1985). Study and interpretation of the chemical characteristics of natural water (Vol. 2254). Department of the Interior, US Geological Survey.

Hideyuki T., Takeshi S., Akira Y. and Takao U (1994). Parameter identification of Two-region model applied to solute transport in sand column breakthrough. Journal of JSCE, 1994 (499): 107-116.

Jackson, R. D., Brizendine, E. J., Kelly, S. A., Hinesley, R., Stookey, G. K., & Dunipace, A. J. (2002). The fluoride content of foods and beverages from negligibly and optimally fluoridated communities. Community dentistry and oral epidemiology, 30(5), 382-391.

Jaremalm, M., Köhler, S., & Lidman, F. (2013). Precipitation of barite in the biosphere and its consequences for the mobility of Ra in Forsmark and Simpevarp (p. 203). SKB report TR-13-28.

Kinniburgh, D. G. (1986). General purpose adsorption isotherms. Environmental science & technology, 20(9), 895-904.

Lapidus, L., & Amundson, N. R. (1952). Mathematics of adsorption in beds. VI. The effect of longitudinal diffusion in ion exchange and chromatographic columns. The Journal of Physical Chemistry, 56(8), 984-988..

Liu, C., & Ball, W. P. (2002). Back diffusion of chlorinated solvent contaminants from a natural aquitard to a remediated aquifer under well-controlled field conditions: Predictions and measurements. Groundwater, 40(2), 175-184.

Maadid, H., Mabrouk, A., & Koulali, Y. (2017). Fluoride content in well waters for human and animal consumption with reported high incidence levels of endemic fluorosis in Beni Meskine (Morocco). Euro-Mediterranean Journal for Environmental Integration, 2(1), 11.

Mondal, N. K., Kundu, M., Das, K., Bhaumik, R., & Datta, J. K. (2013). Biosorption of fluoride from aqueous phase onto *Aspergillus* and its calcium-impregnated biomass and evaluation of adsorption kinetics. Fluoride, 46(4), 239-245.

Murray J.J. [Ed.] 1986 Appropriate Use of Fluorides for Human Health, World Health Organization, Geneva.

Nagendra Rao, C. R. (2003, December). Fluoride and environment-a review. In Proceedings of the third international conference on environment and health, Chennai, India (pp. 15-17).

Nawlakhe, W. G., & Bulusu, K. R. (1989). Nalgonda techniquea process for removal of excess fluoride from water. Water Quality Bull, 14, 218-220.

Ogata, Akio. "A solution of the differential equation of longitudinal disersion in porous media, US." Geological survey professional (1961): paper411-A.

Ozsvath, D. L. (2009). Fluoride and environmental health: a review. Reviews in Environmental Science and Bio/Technology, 8(1), 59-79.

Padhi, S., & Tokunaga, T. (2018). Surface Complexation Modeling of Fluoride Adsorption by

Soil and the Role of Dissolved Aluminum on Adsorption. *Vadose Zone Journal*, 17(1), 1-14.

Parkhurst, D. L., & Appelo, C. A. J. (1999). User's guide to PHREEQC (Version 2): A computer program for speciation, batch-reaction, one-dimensional transport, and inverse geochemical calculations. *Water-resources investigations report*, 99(4259), 312.

Parkhurst, D.L., and Appelo, C.A.J., (2013), Description of input and examples for PHREEQC version 3—A computer program for speciation, batch-reaction, one-dimensional transport, and inverse geochemical calculations: U.S. Geological Survey Techniques and Methods, book 6, chap. A43, 497 p., available only at <http://pubs.usgs.gov/tm/06/a43/>.

Perkins, T. K., & Johnston, O. C. (1963). A review of diffusion and dispersion in porous media. *Society of Petroleum Engineers Journal*, 3(01), 70-84.

Pickering, W. F. (1985). The mobility of soluble fluoride in soils. *Environmental Pollution Series B, Chemical and Physical*, 9(4), 281-308.

Polomski, J., Flühler, H., & Blaser, P. (1982). Fluoride-Induced Mobilization and Leaching of Organic Matter, Iron, and Aluminum. *Journal of Environmental Quality*, 11(3), 452-456.

Rao, P. S. C., Davidson, J. M., Jessup, R. E., & Selim, H. M. (1979). Evaluation of conceptual models for describing nonequilibrium adsorption-desorption of pesticides during steady-flow in soils. *Soil Science Society of America Journal*, 43(1), 22-28.

Rao, P. S. C., Rolston, D. E., Jessup, R. E., & Davidson, J. M. (1980). Solute transport in aggregated porous media: Theoretical and experimental evaluation. *Soil Science Society of America Journal*, 44(6), 1139-1146.

Rea, R. E., & RE, R. (1979). A rapid method for the determination of fluoride in sewage sludges.

Ribeiro, A. C., Lobo, V. M., Sobral, A. J., Soares, H. T. C., Leal, A. R., & Estes, M. A. (2010). Diffusion Coefficients of Sodium Fluoride in Aqueous Solutions at 298.15 K and 310.15 K. *Acta Chim. Slov*, 57, 410-414.

Richards, L. A., Vuachère, M., & Schäfer, A. I. (2010). Impact of pH on the removal of fluoride, nitrate and boron by nanofiltration/reverse osmosis. *Desalination*, 261(3), 331-337.

Roelandts, I., Robaye, G., Weber, G., Delbrouck, J., & Duchesne, J. (1987). Determination of fluorine by proton-induced gamma-ray emission (PIGE) spectrometry in igneous and metamorphic charnockitic rocks from Rogaland (SW Norway). *Journal of Radioanalytical and Nuclear Chemistry*, 112(2), 453-460.

Sakambari Padhi (2015). Reactive transport and adsorption-desorption processes of fluoride in a granitic soil (Doctor's dissertation) The University of Tokyo, Japan

Shulman, J. D., & Wells, L. M. (1997). Acute fluoride toxicity from ingesting home-use dental products in children, birth to 6 years of age. *Journal of public health dentistry*, 57(3), 150-158.

Singh, Gayatri, et al. "Fluoride distribution and contamination in the water, soil and plants continuum and its remedial technologies, an Indian perspective—a review." *Environmental*

Pollution 239 (2018): 95-108.

Smedley, P. L., Nicolli, H. B., Macdonald, D. M. J., Barros, A. J., & Tullio, J. O. (2002). Hydrogeochemistry of arsenic and other inorganic constituents in groundwaters from La Pampa, Argentina. *Applied geochemistry*, 17(3), 259-284.

Smith, F. A., Hodge, H. C., & Dinman, B. D. (1977). Airborne fluorides and man: Part I. Critical Reviews in Environmental Science and Technology, 8(1-4), 293-371.

Stumm, W. (1992). Chemistry of the solid-water interface: processes at the mineral-water and particle-water interface in natural systems. John Wiley & Son Inc..

Tekle-Haimanot, R., Melaku, Z., Kloos, H., Reimann, C., Fantaye, W., Zerihun, L., & Bjorvatn, K. (2006). The geographic distribution of fluoride in surface and groundwater in Ethiopia with an emphasis on the Rift Valley. *Science of the Total Environment*, 367(1), 182-190.

Toride, N., Leij, F. J., & Van Genuchten, M. T. (1995). The CXTFIT code for estimating transport parameters from laboratory or field tracer experiments (Vol. 2). Riverside, CA: US Salinity Laboratory.

Valocchi, A. J., Street, R. L., & Roberts, P. V. (1981). Transport of ion-exchanging solutes in groundwater: Chromatographic theory and field simulation. *Water Resources Research*, 17(5), 1517-1527.

Van Genuchten, M. T., & Wierenga, P. J. (1976). Mass transfer studies in sorbing porous media I. Analytical solutions. *Soil science society of america journal*, 40(4), 473-480.

Van Genuchten, M. T., & Wierenga, P. J. (1977). Mass transfer studies in sorbing porous media: II. Experimental evaluation with tritium ($^3\text{H}_2\text{O}$). *Soil Science Society of America Journal*, 41(2), 272-278.

Van Genuchten, M. Th, and R. J. Wagenet. "Two-site/two-region models for pesticide transport and degradation: Theoretical development and analytical solutions." *Soil Science Society of America Journal* 53.5 (1989): 1303-1310.

Wang, S. X., Wang, Z. H., Cheng, X. T., Li, J., Sang, Z. P., Zhang, X. D., ... & Wang, Z. Q. (2007). Arsenic and fluoride exposure in drinking water: children's IQ and growth in Shanyin county, Shanxi province, China. *Environmental health perspectives*, 115(4), 643-647.

Whitford, G. M., & Pashley, D. H. (1984). Fluoride absorption: the influence of gastric acidity. *Calcified tissue international*, 36(1), 302-307.

World Health Organization. (2002). Environmental health criteria 227: fluorides. World Health Organization, Geneva.

Yang, M., Annable, M. D., & Jawitz, J. W. (2015). Back diffusion from thin low permeability zones. *Environmental science & technology*, 49(1), 415-422.

Yeh, G. T., & Tripathi, V. S. (1989). A critical evaluation of recent developments in hydrogeochemical transport models of reactive multichemical components. *Water resources*

research, 25(1), 93-108.

Young, D. F., & Ball, W. P. (1994). A priori simulation of tetrachloroethene transport through aquifer material using an intraparticle diffusion model. *Environmental progress*, 13(1), 9-20.

Young, D. F., & Ball, W. P. (1995). Effects of column conditions on the first-order rate modeling of nonequilibrium solute breakthrough. *Water Resources Research*, 31(9), 2181-2192.

Šimůnek, J., & van Genuchten, M. T. (2008). Modeling nonequilibrium flow and transport processes using HYDRUS. *Vadose Zone Journal*, 7(2), 782-797.